Fall 12-11-2019

A Climatology of Snowpack in the Southern Rocky Mountains and Snow to Liquid Ratio Forecasting Techniques Using Model Generated Soundings from the Rapid Refresh Model

Carson Jones
University of Nebraska - Lincoln, carson.jones7@huskers.unl.edu

A CLIMATOLOGY OF SNOWPACK IN THE SOUTHERN ROCKY MOUNTAINS AND SNOW TO LIQUID RATIO FORECASTING TECHNIQUES USING MODEL GENERATED SOUNDINGS FROM THE RAPID REFRESH MODEL

by

Carson M. Jones

A THESIS

Presented to the Faculty of

The Graduate College at the University of Nebraska

In Partial Fulfillment of Requirements

For the Degree of Master of Science

Major: Earth and Atmospheric Sciences

Under the Supervision of Professor Mark R. Anderson

Lincoln, Nebraska

December 2019

A CLIMATOLOGY OF SNOWPACK IN THE SOUTHERN ROCKY MOUNTAINS AND SNOW TO LIQUID RATIO FORECASTING TECHNIQUES USING MODEL GENERATED SOUNDINGS FROM THE RAPID REFRESH MODEL

Carson M. Jones, M.S.

University of Nebraska, 2019

Advisor: Mark R. Anderson

Mountainous snowpack represents up to 70% of the total water resources for areas in the western United States. Temperature and precipitation control the accumulation and ablation of the snowpack throughout the cold season, both of which are subject to a changing climate. This study will use a network of snow telemetry (SNOTEL) stations to investigate changes in the snowpack season, snow water equivalent (SWE), and temperature in the southern Rocky Mountain region. Additionally, this study will use model generated soundings from the Rapid Refresh (RAP) model to establish relationships between the depth and cloud proportion of ice crystal growth layers, and the SNOTEL measured snow-to-liquid ratio (SLR). Results indicate that mountain ranges within northern New Mexico and southern Colorado have measured a statistically significant decrease in the length of the snowpack accumulation season, an earlier date and lessened magnitude of maximum SWE, and shortened overall snowpack season length. Northern mountain ranges within the study region also measured a decrease, although to less of an areal extent than ranges in the south. The majority of SNOTEL stations throughout the region measured an increase in both the number and percentage of

days with maximum temperatures above 0 °C. Results from the SLR analysis indicate a higher proportion of the cloud with temperatures colder than -12 °C tended to have higher SLR than those with a high cloud proportion in warmer temperatures. Analysis of the depth of the ice crystal growth layers showed little differentiation in measured SLRs due to the confines of observed lapse rates within snowstorms. Additionally, average and high SLRs were more common with the presence of the dendritic growth layer within the cloud.

Table of Contents

Chapter 1: INTRODUCTION

The Southern Rocky Mountains are a vast expanse of mountainous terrain found in the central third of Colorado, northern New Mexico, and southern Wyoming. Elevation ranges from 1980 m (6500 ft) to 4390 m (14,390 ft) and includes the highest point in the conterminous United States with Mount Elbert measuring 4400 m (14,433 ft) in central Colorado. The region features the Continental Divide and is home to the headwaters of the North and South Platte, Arkansas, and Rio Grande Rivers flowing east and the Green, Yampa, and Colorado Rivers flowing west. The average annual precipitation ranges widely from 17.8 cm (7 in) in the semi-arid region of the Colorado River Plateau to 160 cm (63 in) in the highest elevations of central Colorado. Most averages fall between 35.6 cm (14 in) and 81.3 cm (32 in) in the middle and upper elevations of the high terrain. Throughout the region, about half of the annual precipitation occurs in solid form as snow in the fall, winter, and springs months, with an increasing proportion falling as snow with increasing elevation (USDA 2006). The importance of snowpack to water resources within the region are paramount, with the natural storage capabilities of snowpack often exceeding the storage capacity of humanmade reservoirs (Nijssen et al. 2001). Approximately 70% of all streamflow originates from snowpack melt during the spring and summer months (Avanzi et al. 2015). Changes in snowpack magnitude or melt timing of snowpack subsequently cause changes in storage strategies and dam management during the dry, summer months when the water is most needed for agriculture, drinking, industry, and the maintenance of fragile ecosystems downstream.

Snowpack is commonly measured as snow water equivalent (SWE) to accurately resolve the total amount of water within the snowpack for river and stream basins. The accumulation, persistence, and melt of snowpack is dependent on many factors, primarily precipitation and air temperature. Temperature within the snowpack itself is also very important, although difficult and seldom measured. Snowpack has a wide range of temperatures within the pack, which are a function of the temperature of the snow during the precipitation events, exposure to air temperature fluctuations, and heating from the ground surface. Melt only occurs once a layer of the snowpack is isothermal at 0 °C. Until this occurs, layers within the snowpack colder than 0 °C will refreeze water draining through the snowpack that may have melted at the surface. After a complex process of latent heat exchange and snowpack ablation, the entire snowpack can then melt upon reaching 0 °C throughout its depth. As a result, variability in air temperature, wind, and snow temperature upon precipitation play an important role in the duration of the snowpack season (Pigeon and Jiskoot 2008).

The accumulation of snowfall events each cold season are often reflected in the magnitude of maximum SWE and the timing at which this occurs. After the date of maximum SWE is reached, commonly referred to as the 1 April snowpack, the ablation season begins; however, snowfall events during the ablation season are common and extend the length of the ablation season should they occur. Rain on snow events are very rare in the southern Rocky Mountains and usually occur only towards the beginning and end of the snowpack season. These events accelerate melt by adding a warm water influx to the snowpack (Marks et al. 1998). The start of the accumulation season, also known as the snowpack onset, is highly dependent on the timing of the first substantial snowfall

and the air temperature near the timing of this event. If it is cold enough, the snowpack will begin to form and persist throughout the cold season; however, if the ambient air temperature is too high, the early snowfall event will ablate, and the onset of the snowpack accumulation season will be delayed (Knowles et al. 2006). Runoff from snowmelt is difficult to predict due to the high variability in snowpack temperature between river basins due to factors like aspect, vegetation, ground type, and elevation. Forecasts of runoff commonly use maximum SWE, the date of maximum SWE, and typical ablation timing and duration estimates to predict the peak runoff volume and timing (Clow 2009). Therefore, knowledge of these metrics is crucial to streamflow modeling during the ablation season.

Reductions in maximum SWE observed from 1949 to 2004 have been attributed to earlier snowmelt, later onset of the snowpack season, earlier date of maximum SWE, and more precipitation falling as rain during the tail ends of the cold season, all of which can be directly attributed to variations or increases in temperature (Knowles et al. 2006). Studies conducted in Colorado from 1978 to 2007 have shown that the date of maximum SWE has occurred on average two to three weeks earlier in the season, with a reduction in magnitude of 4.1 to 3.6 cm decade $^{-1}$ (Clow 2009). These losses and earlier ablation season timing have led to decreased streamflow and increased fire danger in the late summer and early fall months for many of the major river basins that originate in Colorado, New Mexico, and southern Wyoming.

Snowpack also provides a major economic asset to the Colorado and New Mexico ski tourism industry. Within the southern Rocky Mountains there are 23 ski resorts in Colorado and 9 in New Mexico. Estimates indicate that Colorado's ski tourism industry

generates approximately $4.8 billion in annual economic impact and supports more than 46,000 full and part-time jobs in recreation, lodging, food services, retail and other sectors, for an estimated $1.9 billion per year in labor income. Approximately 500,000 Coloradans and an estimated seven million visitors utilize Colorado's ski industry each year (Colorado Ski Country USA 2015). In New Mexico, skiing represents one of the largest contributors to the tourism economy as well, with an economic impact of approximately $421 million in 2016. A poor winter season in 2017 cost the ski tourism industry approximately $123 million due to a late season opening and early season closing (Albuquerque Business First 2018). To combat climate change, low snowfall seasons, and the growing demand for early season skiing, Vail Ski Resorts, North America's largest ski conglomerate, has invested over $1.2 billion into new snowmaking techniques and improved lift access (Vail Resorts 2018) across 17 of their North American ski resorts. High elevation resorts, particularly those found in Colorado, have a comparative advantage over lower ski areas in the ability to achieve optimum snowmaking temperatures of 0.0 °C to -5.0 °C (Bark 2009). This has resulted in large snowmaking investments by the Colorado and New Mexico ski industry.

The primary purpose of this study is to investigate changes in snowpack metrics throughout the southern Rocky Mountain region. This study will build upon the findings of previous studies conducted by Clow (2009), Mote et al. (2004), and McCabe and Dettinger (2002). Snowpack metrics include variables such as season length, maximum SWE, and the date of maximum SWE. These metrics will be analyzed over a 30 to 40-year period beginning in 1979 and ending in 2018. Changes in SWE will be ascribed to changes in temperature and total precipitation during the cold season. Statistical

analyses will be conducted to identify changes in SWE metrics over time. Although SWE is very important from a water resources perspective, the snow depth of individual snowfall events is important to many industries in mitigation or utilization of snowfall for their industries' practice. Snow depth also affects the general public in day-to-day transportation and activities. Operational forecasting often fails to correctly diagnose the snow-to-liquid ratio (SLR) for snowfall events. The secondary purpose of this study is to provide a helpful tool to diagnose SLR in mountainous terrain. To accomplish this, modeled soundings will be derived from the Rapid Refresh (RAP) Numerical Prediction Model and relationships between the depth of ice crystal growth temperature regimes and SLR will be established.

CHAPTER 2: BACKGROUND

2.1. Snowpack, SWE, and SNOTEL

Snowpack has many methods of measurement in mountainous terrain, varying from human measurement from trained observers to automated stations in remote areas. The most common method for snowpack measurement in the western United States is the snow telemetry (SNOTEL) network. Beginning in the 1960's, remote stations were installed throughout the west to test the ability to measure SWE in remote and low traffic regions within mountainous terrain. By 1979, SNOTEL stations were rapidly established in the large mountain valleys and ridges, which feed many of the nation's largest river basins. SNOTEL stations were originally designed to solely measure SWE using a snow pillow, which derives SWE based on the weight of the snowpack above it. Changes in air pressure within the pillow are then ascribed to a SWE amount. Beginning in 1985, SNOTEL stations were retrofitted as weather stations, measuring temperature, wind speed and direction. To establish the depth of the snowpack, downward pointing sonic sensors were installed beginning in the early 2000's. Originally, SWE data were measured each day at midnight with hourly data availability beginning in the mid-1990's (USDA 2017).

Of primary importance for the SNOTEL network is to measure the 1 April SWE (hereafter max SWE). This term is commonly used to represent the maximum SWE, or water available for the spring and summer ablation season, although the actual date of max SWE varies greatly by region and elevation (Cayan 1996). The availability of

continuous, automated SWE measurement beginning in 1980 allows for dependable data devoid of human inconsistencies in estimation and measurement error. However, automated systems like SNOTEL do still have errors. Measurement errors with solid precipitation gauges used by the National Weather Service (NWS) and World Meteorological Organization (WMO) often range from 20% to 50% due to wind, wetting, gage blocking, and sensor sensitivity (Rasmusen et al. 2012). These errors are not as common for SNOTEL stations SWE measurements due to the below ground positioning of the snow pillow; however, long term consistency of the site, although well preserved, may see changes in the environment due to variations in the forest canopy, forest encroachment, and nearby ground surface changes (Mote et al. 2005).

Long term climatological studies have come to a consensus that the snowpack has been decreasing throughout much of the western United States over the last century. Data from snow course sites, SNOTEL sites, and most recently NASA's Airborne Snow Observatory, have shown an earlier date of max SWE and a later onset of the snowpack accumulation season (Mote et al. 2005, McCabe and Dettinger 2002). Nationally, there has been an observed decrease in the number of days with snow on the ground and less total annual snowfall when comparing the 1971-2000 and 1981-2010 climate averaging periods (Durre et al. 2013). The cause of the decline, however, is not uniform throughout the western United States due to variance in the effect of temperature and precipitation on snowpack. Many areas of the Pacific Northwest and northern California have observed a slight increase in precipitation over high-elevation areas over the last century; however, anticipated increases in SWE that should accompany an increase in precipitation have not been observed due to a warming trend, shorter cold season, and an increase in the

proportion of cold season precipitation falling as rain rather than snow. Decreases in SWE in areas of the Rocky Mountains and southern Sierra Nevada are less attributable to temperature trends and more a function of a decrease in precipitation (Hamlet et al. 2005). Future snowfall and SWE has also been numerically modeled using long range climate models. Studies conducted through the end of the 21st century indicate a decrease in snowfall and SWE by up to 50% in some areas of the Colorado River Basin, particularly high elevation areas in the southern part of the basin and low elevation areas in the northern part of the basin (Wi et al. 2012).

2.2 SLR

Of interest to operational forecasting is the SLR. The common rule of thumb for SLR forecasting is the "ten-to-one rule (10:1)," which is based on an early nineteenth century estimate of 10 inches (25.4 cm) of measured snow accumulation to 1 inch (2.54 cm) in SWE in Toronto, Canada (Power 1965). However, actual measurements of SLR vary greatly between storm systems and locations. The societal impact of misdiagnosing the SLR as 10:1, when it is actually 3:1 or 60:1, can cause major problems as the actual depth of new snow is what is experienced by drivers, skiers, road and airport maintenance crews, and avalanche mitigation experts. In fact, SLR can range by as much as 2:1 to 100:1 throughout the continental United States (Judson and Doesken 2000). In the southern Rockies, mean SLR ranges from 14:1 in northern New Mexico to 16:1 in southern Wyoming with measurements in the 20th and 75th percentiles between 10:1 and 19:1, respectively. Most of the variability in SLR ratios within the region are due to

elevational and geographic differences with higher, northern locations receiving a higher SLR than lower, southern locations (Baxter et al. 2005). Although correct SLR estimation is very important to operational forecasting, it remains one of the lowest skill metrics for operational forecasters (Alcott and Steenburgh 2010).

High variability and low forecasting skill for SLR is a function of the complex nature in which ice crystals form, fall, and deposit on the ground. Ice crystals may begin to form between -10.0 °C and 0.0 °C, although observations are very rare due to the low availability of ice nuclei present for activation in this "warm" temperature range. As temperature decreases, more ice nuclei are likely to become activated and more ice crystals subsequently form. Crystal type varies widely in each storm and throughout different regions of the world. Studies have observed over 80 different types of ice particles, which differ in size, shape, axis ratio, and the presence of dendritic arms (Bailey and Hallett 2004 and 2009). In their most basic form, ice crystals in the atmosphere are commonly divided into four categories: needles, columns, plates, and dendrites, each with different density and SLR (Stoelinga 2003). Once the ice crystals reach the ground surface, the particles containing dendritic arms are generally measured to be the least dense due to the air space between the outwardly extending arms of the ice crystal. Dendritic arms also can grow the largest out of all the other crystal types due to the high surface area of the crystal. Upon accumulation at the ground, dendritic crystals will maintain the large amount of air between the outwardly branching arms, which leads to the accumulation of air filled, or less dense snow, and therefore a higher SLR. Density typically increases from plates to columns to needles, with needles containing the highest snow density of the four crystal types. This is due to how crystals lay upon reaching the

ground surface, with needles being the longest and thinnest of the crystal types, laying with the longest axis most commonly parallel to the ground surface. When the needles accumulate, they will tend to stack up with little air space between the ice crystals (Judson and Doesken 2000).

Atmospheric ice crystal growth is primarily a function of temperature and secondarily a function of moisture. The basic ice crystal habits and formation temperatures are represented within Table 2.1. Although growth of these basic ice crystal categories is common within the specified temperature regimes, ice crystal diversity is high in each snowstorm and crystals may undergo metamorphosis in both the atmosphere and at the surface, which will change the shape and density of the crystals over time (Fukuta and Takahashi 1999). Of interest is the dendritic growth zone, where the difference in degree of water vapor saturation over ice is greatest compared to vapor saturation over water. This causes rapid growth of low density, large (dendritic) ice crystals (McCormick 2009). Moisture within ice crystal growth layers is also important. A study in the Wasatch Mountains indicated that within high magnitude SWE storms, greater levels of moisture in the mid- and upper levels lead to lower SLR's due to slow crystal growth rates of lower density ice crystals at colder temperatures. The level of relative humidity showed no clear correlation to SLR in lower, warmer layers of the atmosphere (Alcott and Steenburgh 2010).

Table 2.1. Temperature range and respective dominate type of ice crystal.

	Temperature Range (°C)						
	0 to -3	-3 to -6	-6 to -10	-10 to -12	-12 to -16	-16 to -22	-22 to -30
Crystal Type	Thick Plates	Needles	Hollow Columns	Stellar Plates	Dendrites	Large Plates	Columns

Judson and Doesken (2000) investigated ice crystal habits within the cloud and subcloud, where ice crystals are subject to sublimation, riming, melting, and fragmentation. Sublimation can occur when ice crystals fall through a layer that is subsaturated and tends to decrease the size of outwardly branching ice crystal arms, thus increasing the density of the ice crystal upon contact with the surface. Riming will occur at temperatures warmer than -15.0 °C with the greatest amount of riming occurring at temperatures warmer than -10.0 °C due to the high amounts of supercool water droplets. Riming typically acts to fill ice crystal branches without adding to the overall size of the ice crystal, which will increase its density. Melting also increases the density of the ice crystal and will occur if the crystal falls through a warm layer (T > 0.0 °C). Fragmentation occurs when snow crystals collide, break, and fail to coalesce, which acts to increase the density by allowing more, smaller ice crystals to accumulate on the surface.

At the surface, ice crystal metamorphosis can occur via wind fragmentation and compaction, melting, compaction via the weight of overlying snow, and ageing. Surface wind speeds greater than 9 m s^{-1} causes ice crystals on the top snow layer to fracture in a process known as sintering (Baxter et al. 2005). Although sintering can act to remove some crystal fragments from the snowpack, it also causes compaction by forcing crystals to arrange tighter together, thus increasing the density of the near surface layer. Surface melting will increase the snow density by changing the crystal structure to form pellet like ice structures known as facets. These small, round faceted ice crystals are both large and high in water content as melting acts to bring water towards the center of the ice crystal (McCormick 2009). As snow accumulates, weight from continual snowfall will

act to decrease the accumulation depth over time and increase the density of the snowpack. The rate of compaction is large for snow temperatures near 0.0 °C and decreases by a factor of two for every 6.0 °C decrease in snow temperature (Conway and Wilbur 1999). The processes can all combine on timescales from minutes to days to change the density of the snowpack at the surface. Lastly, ageing is the process by which vapor diffusion transfers mass from convex to concave corners of the ice crystal, creating a round crystal over time. This process occurs on the timescale of days to a season, acting to increase the density within the snowpack over time. The aging process therefore has little effect on SLR measurements taken at the time of snowfall (McCormick 2009).

Although numerical weather prediction of SLR has improved, models still often fail to produce high forecasting skill scores for SLR. Of the current NCEP models, the Rapid Refresh (RAP) shows the highest skill in model initializations for both SWE and snow depth (Dawson et al. 2016). Additionally, when compared to rawinsonde observations conducted twice daily by the NWS, model generated soundings showed an average temperature bias between 0.1 °C and 0.2 °C and an average relative humidity bias of less than -2% across the conterminous United States. As a result, model generated soundings are often slightly warmer and drier than the "truth" measurements from the NWS; however, these errors are small in nature for the 1-hour forecast, thus allowing the RAP generated soundings to be a "best guess" estimate (Benjamin et al. 2015). The RAP also inputs SWE and snow depth data from SNOTEL stations into each model cycle rather than relying on model estimates built into the model itself. To predict the SLR, the RAP first derives a precipitation accumulation amount at each grid point,

which is then converted to either a 10:1 SLR or a variable SLR, which ranges from 5:1 to 13:1 (Benjamin 2019). Even the highest of the variable SLR estimations is well below the climatological mean SLR for the southern Rocky Mountains which ranges from 14:1 to 16:1 (Baxter et al. 2005).

Chapter 3: DATA AND METHODS

The primary goal of this study is to analyze the seasonal snowpack in the Southern Rocky Mountains beginning with the establishment of SNOTEL stations in fall 1979 and ending with the summer of 2018. Analysis will be conducted for SWE amounts, length of the snowpack seasons, the proportion of SWE retained in the snowpack at its peak, and the number of days that the snowpack is subject to ablation during a snowpack season. Variability or change in these metrics over time can be used to assess the stability and utility of snowpack as a major water resource for the region. The secondary goal of the study is to analyze vertical temperature and humidity profiles using the RAP model reanalysis dataset in conjunction with surface SWE, and snow accumulation from the SNOTEL network to better correlate the SLR with varying temperature and moisture profiles in snowstorms.

3.1 SNOTEL Data

3.1.1 Snowpack Climatology

For climatological analysis, daily observations of SWE and maximum air temperatures were obtained from the Natural Resources Conservation Service (NRCS) SNOTEL station archive (USDA 2018). The analysis period will be from 1 October 1979 to 30 June 2018. In total, there are 137 stations throughout the Southern Rocky Mountain region which have been divided into seven mountain ranges consistent with

divisions made within the NRCS. The seven mountain ranges (Figure 3.1) are: Front Range, Park Range, Flat Top Mountains, Central Range, northern and central San Juan Mountains (hereafter San Juan Mountains), Sangre de Cristo Mountains, and the southern San Juan Mountains and Nacimiento Mountains (hereafter Nacimiento Mountains).

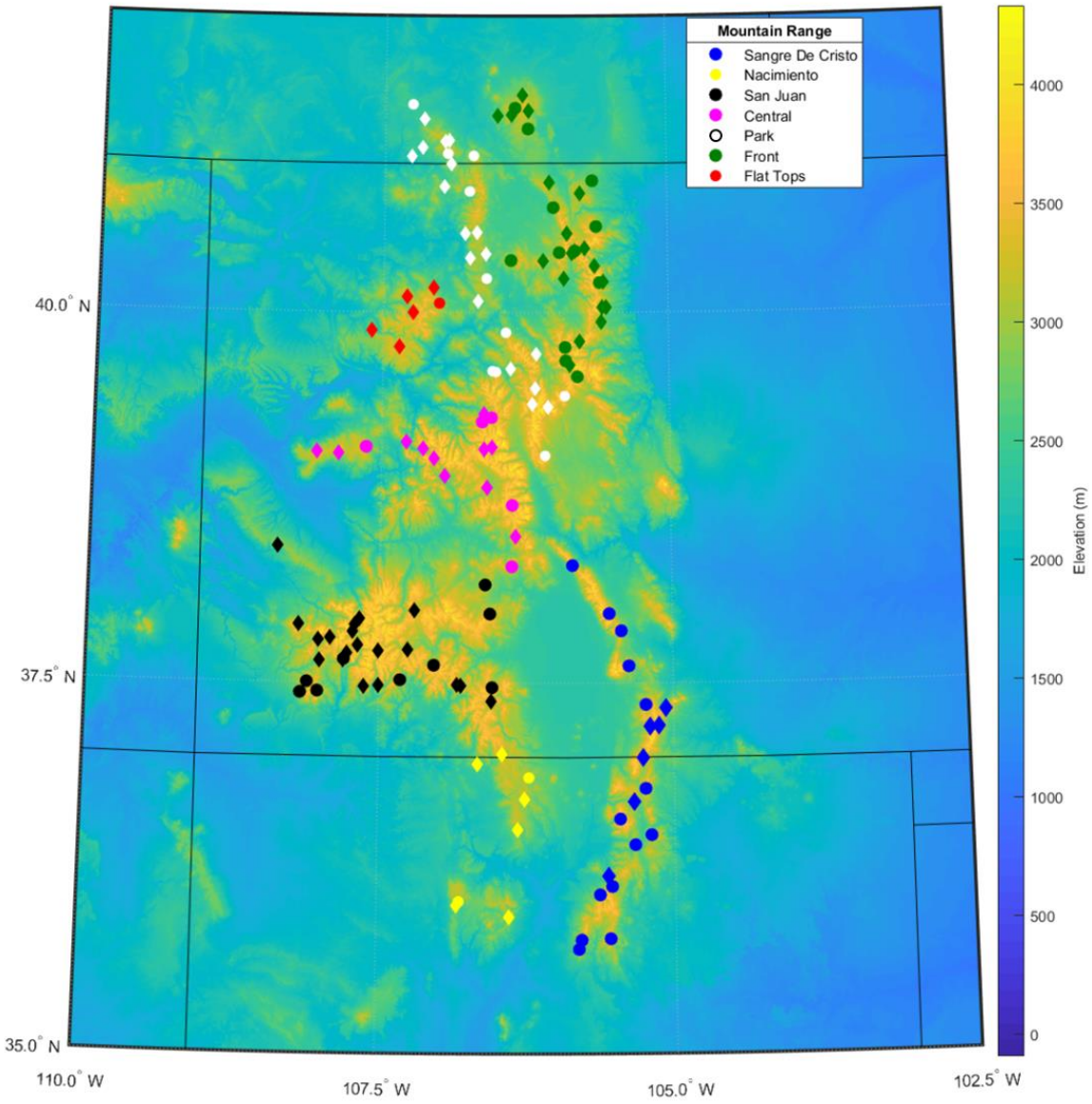

Figure 3.1 Map of snow telemetry (SNOTEL) stations used in this study, grouped by mountain range. Stations used in the snowpack climatology are represented by a diamond.

For the climatological analysis, stations must have at least 30 years of continuous SWE and air temperature data to be considered. In total, there are 85 and 67 SNOTEL stations that match this criterion for SWE and air temperature data respectively (Table 3.1).

The elevation of the SNOTEL stations ranges from 2268 m (7440 ft) to 3542 m (11,620 ft) with a mean of 3040 m (9973 ft) and median of 3057 m (10,030 ft) (Table 3.1). This provides an elevational difference of 1274 m (4180 ft) for the climatology. Station latitudes range from 35.704 °N in northern New Mexico to 41.463 °N in southern Wyoming. Longitudinal variation is less, with the westernmost station at 106.524 °W and easternmost station at 105.067 °W.

Similar to studies conducted by Oaida et al. (2019), and McCabe and Dettinger (2002), the snowpack duration can be defined into two seasons, accumulation and ablation, between which the peak snowpack, or maximum SWE is measured (hereafter max SWE). The date and magnitude of max SWE will be measured for each water year beginning 1 October. The onset of continuous snowpack will be defined as the first date on which snowpack is nonzero for multiple months as to avoid shorter durations of intermittent snowpack or individual snowfall events that ablate shortly thereafter.

Table 3.1. Study area characteristics. n is number of stations in each mountain range, n* is the number of stations used for SWE metric climatology and n** is the number of stations used in the temperature metric climatology.

	Elevation (m)			Latitude (°N)		Longitude (°W)				
Range	Max	Min	Median	Max	Min	Max	Min	n	n*	n**
Front	3493	2572	3084	41.46	38.88	105.07	106.50	31	19	13
Park	3475	2268	2819	41.40	39.03	105.91	107.27	25	16	14
Flat Top	3316	2767	2911	40.17	39.76	107.01	107.60	6	5	5
Central Range	3514	2652	3097	39.86	37.97	106.34	108.06	21	13	11
San Juan	3542	2706	3225	38.42	37.38	106.54	108.38	26	20	19
Sangre De Cristo	3488	2502	3115	38.29	35.70	105.07	106.39	21	6	1
Nacimiento	3097	2560	2835	37.02	36.00	106.23	106.83	7	6	4
Study Area	3542	2268	3057	41.46	35.70	105.07	108.38	137	85	67

The end date of the snowpack season will be defined as the first day on which SNOTEL stations measure zero SWE after max SWE has been reached. The accumulation season will be defined as the length in days from the first date of continuous snowpack until the date of max SWE whereas the ablation season will be defined as the length in days from the date of max SWE until the first day of zero measurement. The number of days of continuous snowpack, the accumulation season, and the ablation season will be counted for each water year for the 85 SNOTEL stations.

Three metrics (hereafter SWE metrics) will be used to quantify the magnitude of SWE for each water year: max SWE, gross SWE, and ablated SWE. Gross SWE incorporates midseason losses due to ablation and possible subsequent gains due to snowfall, or in other words the summation of all SWE increases throughout the season. Ablation incorporates sublimation, melting and evaporation, all of which are highly dependent on the ambient air temperatures (hereafter temperature). To assess changes in the snowpack as a result of ablation, maximum daily temperature data are measured throughout the snowpack season. The number of days that the maximum air temperature exceeds 0.0 °C per season (hereafter known as warm days), will be measured to assess the length of which the snowpack is exposed to ablation processes. The proportion of the number of warm days to the season length (hereafter % warm days) will also be analyzed to normalize the duration that each station is subject to ablation processes.

3.1.2 SLR Data

For the purpose of vertical profile analysis and SLR determination, hourly SWE and snow depth measurements were obtained for the period of 1 January 2014 through 31 December 2018. This time period was chosen because all 137 SNOTEL stations have hourly data after 1 January 2014. SLR is determined by dividing the gross SWE accumulation by the gross change in snow depth over a 3-hour period. SWE and snow depth have a measurement accuracy of 0.25 cm (0.1 in) and 1.27 cm (0.5 in) respectively. However, snow depth is reported to the nearest 2.54 cm (1 in). To determine a date for SLR analysis, 24-hour SWE accumulation is measured at each SNOTEL site. In order to provide as many SLR measurements as possible, dates with SWE accumulation greater than 5.08 cm (2 in) are used. Stations chosen must additionally have at least 25.4 cm (10 in) gross accumulation over the 24-hour period to provide a higher degree of variation in SLR measurements. At least five SNOTEL stations must meet this criterion for the date to be considered for analysis. In total six events were chosen using the criteria presented above.

3.2 RAP Reanalysis Data

The RAP analysis collection dataset was obtained from the NCEI THREDDS data center (NOAA/NCEI 2017). Horizontal model grid point spacing is 13 km with 37 isobaric levels ranging from 1000 hPa to 100 hPa. Model grid point spacing in the

vertical is 25 hPa. The model output is projected onto a 450x336 Lambert Conformal Conic projection. After the timing and the location of the SLR event is chosen, the model grid point closest to the SNOTEL station will be used to assess the atmospheric profile of the event. To generate a model sounding, surface and isobaric temperature, dewpoint, wind speed and wind direction, and geopotential height data were obtained. The zero hour, or model initialization, will be used for analysis with data gathered every 3-hours for the duration of the event. Data will be collected from 0 UTC the day of the event to 6 UTC the day after the event. This is done to ensure that the state of the atmosphere is analyzed in the hours prior to the 24-hour analysis period as well as through the end of the day local time. SNOTEL data are reported using MST/MDT, so data will be converted to UTC time to correctly correlate the timing of the snowfall event with the model sounding. This results in 11 model generated soundings at each location for each event.

3.3 Data Analysis

3.3.1 Climatological Data Analysis

The aim of this study is to detect variations in the snowpack on a yearly basis using simple linear regression. The slope of the relationship will be used to test if increases or decreases of the snowpack, SWE and temperature metrics are statistically significant. The correlation coefficient (R) will be used to test the strength of the linear relationship and the proportion of the variance of the snowpack, SWE and temperature

metrics to time. This analysis will be done for each of the 85 and 67 SNOTEL stations for SWE/snowpack and temperature metrics respectively. Regional and statewide results will also be performed and discussed. Correlation coefficients are then converted to a p-value with the use of a t-statistic. Of interest is whether the p-value differs significantly from zero, an indication that the strength of the linear relationship is sufficiently significant. The cutoff for statistically significant results is set at the 90% confidence interval. The null hypothesis is that the true correlation between the SWE metrics and temperature to time is zero. A large p-value ($p>0.1$) indicates weak evidence against the null hypothesis, yielding that the true correlation is close to zero or that none of the discussed metrics are changing with time. Conversely, as shown in the Bateman SNOTEL station in the Nacimiento Mountains (Figure 3.2), a small p-value ($p<0.1$) rejects the null hypothesis and shows a strong decrease in season length.

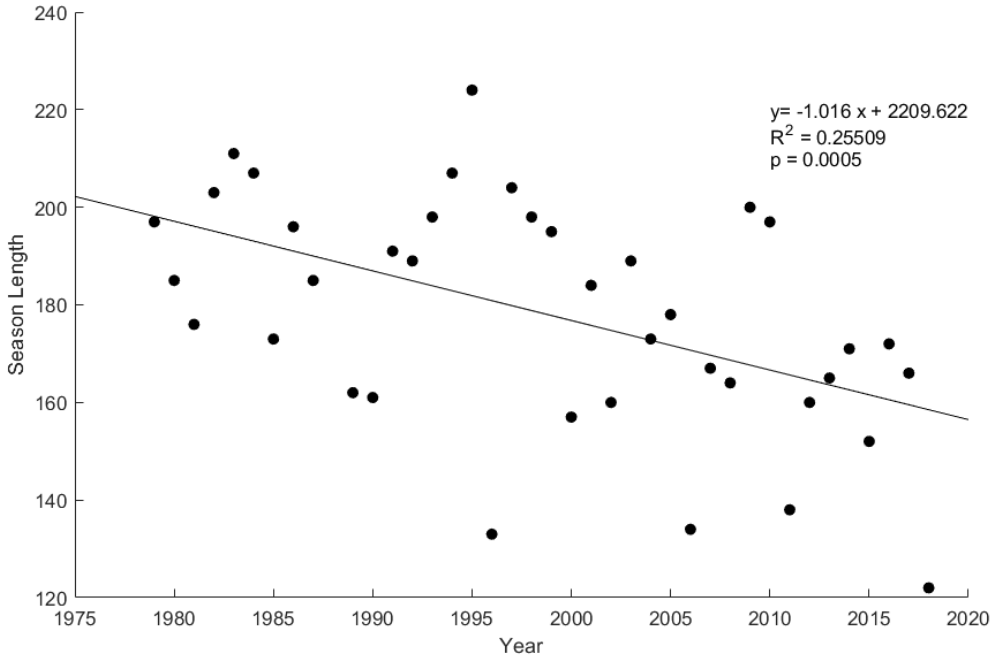

Figure 3.2. Trendline and summary statistics of the season length for Bateman, NM. (USDA/NRCS 2018).

3.3.2 RAP and SLR Data Analysis

Of interest for the SLR analysis is the depth of the snow crystal growth temperature regimes within the atmospheric profile. The depth will be calculated corresponding to the temperature ranges of the ice crystal growth layers (Table 2.1). Larger scale temperature regimes from the surface to -10 °C and -10 °C to -22 °C will also be analyzed (hereafter warm mixed phase layer and cold mixed phase layer respectively). Since the desired temperature is seldom found at each isobaric level, the geopotential height (Z) of each temperature (T) must be interpolated between the isobaric levels presented by the model reanalysis dataset (Figure 3.3). To accomplish this, a simple linear regression, $Z = m*T + h$, is derived. The slope, m, is derived using the temperature (t) and geopotential height (z) of the model isobaric layers, where $m = (z_2 - z_1)/(t_2 - t_1)$, and h is the derived intercept for the equation. Using this equation, the geopotential height of each temperature corresponding to the bounds of ice

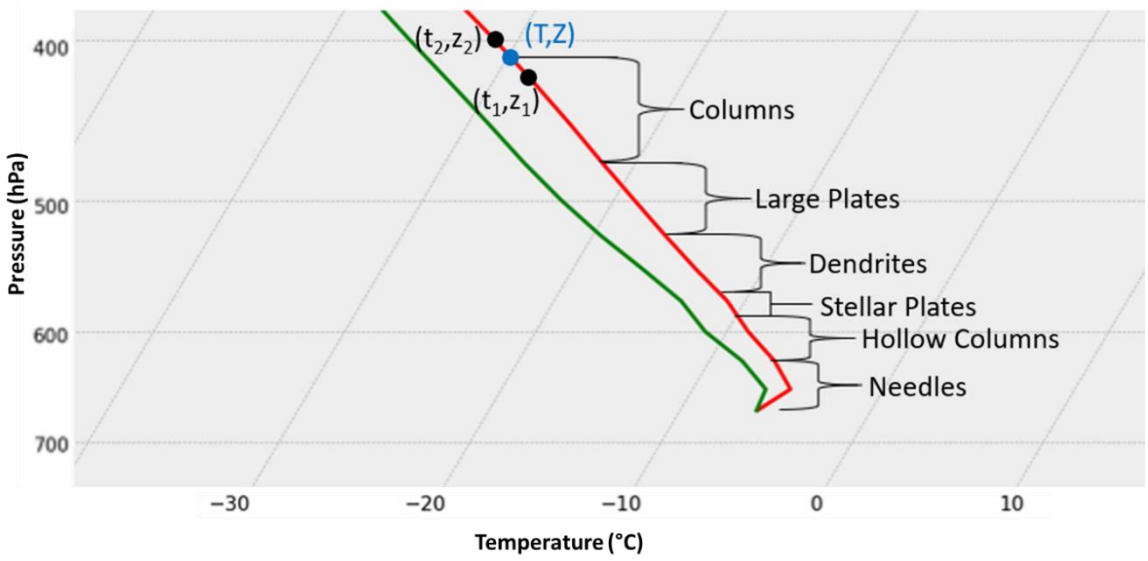

Figure 3.3. RAP generated sounding from Bear Lake, CO. The temperature range of the ice crystal growth layer is encompassed within the brackets.

crystal growth layers is derived. To calculate the depth of the crystal growth layer, simple differencing is applied between the depth of the temperature bounds.

To be considered for analysis, each ice crystal growth layer must be near saturation with respect to water, thus indicating the presence of a cloud layer. A dewpoint depression of 2.5 °C and 5.0 °C (hereafter low DD and high DD) will be applied as a saturation threshold. Layers that do not meet this criterion, regardless of measured snowfall, are omitted from the analysis so that only layers within the saturation threshold are analyzed. By omitting these cases and analyzing the proportion of events that have high DD and low DD to the total number of events, the utility of the using the high and low DD thresholds can be determined. The high DD threshold for below freezing temperatures has a relative humidity greater than 80% for the investigated temperature range (Figure 3.4), which represents a cloud fraction of approximately 75%. The low DD threshold has a relative humidity range of approximately 65% - 70%, representing a cloud fraction of approximately 60% (Giorgio 2017). Due to the excess water vapor pressure with respect to ice throughout the range of temperatures investigated in this study, it is reasonable to assume that ice crystal growth may still occur within the high DD threshold. The depth of each snow growth layer, the proportion of the snow growth layer to the total cloud depth, and the total cloud depth will be evaluated. The total cloud depth is defined as the summation of all individual crystal growth layers that meet the high or low DD threshold. Analysis of the results will be conducted using simple linear regression between SLR and the ice crystal growth depths and cloud proportions. The slope of the regression curve will be discussed, and conclusions will be drawn.

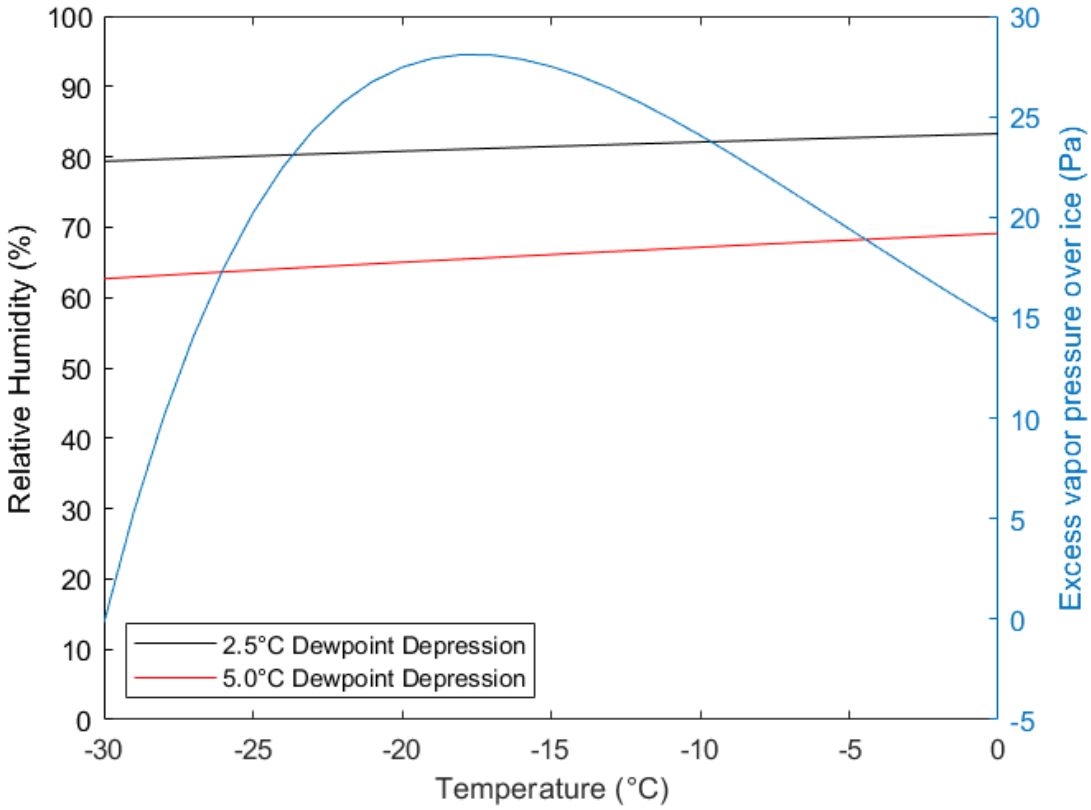

Figure 3.4. Relative humidity over water as a function of temperature and dewpoint depression. Excess vapor pressure over ice (blue line) for the ice crystal growth temperature range.

CHAPTER 4: RESULTS

4.1 Snowpack

Snowpack season metrics relating to the timing of events such as the onset, peak and end dates, as well as the length of the accumulation and ablation seasons, vary by mountain range. Generally, the length of the season decreases from north to south across the mountain ranges (Table 4.1), particularly those equatorward of 38 °N latitude. With the decrease in season length there is also a general decrease in all snowpack season metrics, like length of the accumulation season and an earlier date of max SWE, that are encompassed within the season length. This isn't surprising given the general decrease in temperature with increasing latitude. Colder temperatures in the northern ranges are more likely to prevent early season snow events from ablation, thus providing an earlier mean onset date than the warmer ranges to the south. This results in a shift in the onset date from mid- to late October in the northern ranges to late October and early November onset date in the southern ranges. Variability within the onset date is mostly consistent throughout the study region with a standard deviation (σ) of approximately seven days for most mountain ranges. The Park Range had the highest variation in onset date with a σ of 14 days, which is likely due to the nearly 1200 m (3937 ft) range in station elevations and the high north-south variation of station locations. These two factors allow high stations in the north to receive and retain snow much earlier than their southerly and low elevation counterparts, thus resulting in a highly variable onset date for the Park Range.

Table 4.1. Mean dates for the onset, date of max SWE and last day of the snowpack season; mean length for the accumulation, melting and total length of the snowpack season (days); mean values for max SWE, gross SWE and ablated SWE (cm); mean number of days where the maximum temperature exceeds 0.0°C (warm days) and percent of the season where the maximum temperature exceeds 0.0°C (% warm days). Standard deviations (σ) are calculated for each variable. * The Sangre de Cristo Mountains only have one station that fulfills the requirements for temperature analysis and therefore there is no σ.

	Onset		Max		Last		Accumulation		Ablation		Length		Max SWE		Gross SWE		Ablated SWE		Warm Days		% Warm days	
Range	mean (date)	σ	mean (date)	σ	mean (date)	σ	mean (days)	σ	mean (days)	σ	mean (days)	σ	mean (cm)	σ	mean (cm)	σ	mean (cm)	σ	mean (days)	σ	mean (%)	σ
Front	21 Oct	9	20 Apr	16	1 Jun	18	180	25	41	5	221	29	49	21	59	21	10	3	129	13	61	9
Park	24 Oct	14	15 Apr	14	27 May	17	173	22	42	6	215	25	59	26	68	27	9	2	132	9	62	8
Flat Top	25 Oct	7	15 Apr	11	30 May	19	172	17	44	8	216	25	56	18	66	18	9	1	141	5	66	8
Central	28 Oct	7	11 Apr	10	22 May	13	166	16	40	6	206	20	49	20	60	22	9	2	140	10	67	4
San Juan	27 Oct	10	4 Apr	14	18 May	16	155	23	44	6	199	25	49	17	60	17	10	3	143	11	74	6
Sangre De Cristo	7 Nov	8	23 Mar	6	28 Apr	10	135	12	36	4	171	15	26	7	36	6	10	3	122*	N/A	74*	N/A
Nacimiento	2 Nov	6	23 Mar	12	30 Apr	16	136	21	38	5	174	25	38	19	45	20	7	1	127	17	76	12
Study Area Average	28 Oct	9	7 Apr	12	18 May	16	160	19	41	6	200	23	47	18	56	19	9	2	135	11	68	8

The mean date of max SWE shows variation of close to one month between the northern and southern ranges with the Front Range having a mean date of 20 April and the two ranges within New Mexico, the Nacimiento, and Sangre de Cristo Mountains, having a mean date of 23 March (Table 4.1). This is likely the result of a higher percentage of days within the snowpack season having a high temperature above 0 °C. In fact, the number of warm days for the southern mountain ranges is very similar to the number of warm days in the northern ranges despite the total season length being shorter. The higher proportion of warm days allows the snowpack to condition itself for ablation in the southern ranges much earlier than the northern ranges, resulting in an earlier date of max SWE in the southern ranges. The smaller proportion of warm days in the northern ranges keeps the snowpack colder throughout the season, allowing it to continue to accumulate without substantial ablation later into the season.

The end date for the snowpack season also shows an approximately one-month delay from the northern ranges to the southern ranges ranging from late April to late May (Table 4.1). The San Juan Mountains do retain snowpack for longer than the Nacimiento and Sangre de Cristo Mountains as a result of being slightly higher in elevation and receiving more snowfall. The rate of ablation for the snowpack is overall consistent throughout all the mountain ranges, with an average rate of decrease of 2.82 cm day^{-1} (1.11 in day^{-1}) with a σ of 0.5 cm day^{-1} (0.2 in day^{-1}).

The magnitude of SWE metrics such as max SWE, gross SWE and ablated SWE show high variability throughout the mountain ranges and within each range (Table 4.1). For example, the Park Range shows an approximately 26.5 cm (10.2 in) σ in max SWE and gross SWE, which indicates high inter-annual and inter-area variability in snowpack.

The ablated SWE is consistent throughout the study region with a mean of 9 cm (3.5 in) even though the percentage of warm days increases in the equatorward direction. This may seem contradictory; however, the longer accumulation season in the northern mountain ranges provides a longer period for ablation, thus allowing the total ablation to be similar throughout the study area. Although the mean ablated SWE shows little variation, the proportion of the gross SWE lost to ablation is disproportionately high in the Sangre de Cristo Mountains. With a mean max and gross SWE of only 26 cm (10.2 in) and 36 cm (14.2 in) respectively, approximately 28% of the gross SWE in the Sangre de Cristo Mountains is lost to ablation while the other mountain ranges lose only approximately 15%. Thus, the Sangre de Cristo Mountains loses a disproportionately high amount of snowpack to ablation during the accumulation season.

The tendency for many of the mountain ranges is toward a shorter accumulation season, earlier date of max SWE, and greater ablated SWE (Table 4.2) with mean study area values of 51%, 55% and 55% respectively. The geographic trend for mountain ranges with a shorter accumulation season and an earlier date of max SWE follows the same north-south distribution as the mean snowpack season and SWE metrics (Table 4.1). The length of the ablation season indicates little change throughout the study area except for the Front and Park Ranges with 26% and 25% of stations measuring an increase respectively. Additionally, 16% and 6% of stations in the Front and Park Ranges also measure statistically significant increases in gross SWE, which indicates that increased total snowfall during the ablation season, and an earlier date of max SWE, could be resulting in a longer ablation season for the two mountain ranges. Similar increases in the length of the ablation season are observed in the Central and San Juan

Mountains, although the number of stations represent only 8% and 10% of each area respectively.

Table 4.2. Percentage of stations within each mountain range with (a) positive or (b) negative r-values that are statistically significant at the 90% confidence level for snowpack season metrics, SWE metrics and temperature metrics. The number of stations within each mountain range meeting the significance level are given within the parenthesis.

a. Positive r-value percentages and frequencies.

	Snowpack Season Metrics				SWE metrics			Temp. Metrics	
Range	Acc.	Max	Ablation	Length	Max	Gross	Ablation	Warm Days	% Warm Days
Front	0 (0)	5 (1)	26 (5)	0 (0)	5 (1)	16 (3)	63 (12)	77 (10)	92 (12)
Park	0 (0)	0 (0)	25 (4)	6 (1)	0 (0)	6 (1)	56 (9)	57 (8)	93 (13)
Flat Top	0 (0)	0 (0)	0 (0)	0 (0)	0 (0)	0 (0)	80 (4)	40 (2)	40 (2)
Central	0 (0)	0 (0)	8 (1)	0 (0)	0 (0)	0 (0)	62 (8)	45 (5)	55 (6)
San Juan	0 (0)	0 (0)	10 (2)	0 (0)	0 (0)	0 (0)	40 (8)	42 (8)	72 (15)
Sangre De Cristo	0 (0)	0 (0)	0 (0)	0 (0)	0 (0)	0 (0)	67 (4)	100 (1)	100 (1)
Nacimiento	0 (0)	0 (0)	0 (0)	0 (0)	0 (0)	0 (0)	40 (2)	75 (3)	100 (4)
Study Area Average	0 (0)	1 (1)	18 (12)	1 (1)	1 (1)	5 (4)	55 (47)	55 (36)	79 (53)

b. Negative r-value percentages and frequencies.

	Snowpack Season Metrics				SWE metrics			Temp. Metrics	
Range	Acc.	Max	Ablation	Length	Max	Gross	Ablation	Warm Days	% Warm Days
Front	32 (6)	26 (5)	5 (1)	21 (4)	5 (1)	0 (0)	0 (0)	0 (0)	0 (0)
Park	44 (7)	44 (7)	0 (0)	31 (5)	19 (3)	0 (0)	0 (0)	7 (1)	0 (0)
Flat Top	40 (2)	20 (1)	0 (0)	40 (2)	60 (3)	50 (3)	0 (0)	0 (0)	0 (0)
Central	62 (8)	80 (10)	0 (0)	54 (7)	15 (2)	15 (2)	0 (0)	18 (2)	0 (0)
San Juan	65 (13)	70 (14)	0 (0)	50 (10)	65 (13)	50 (10)	0 (0)	11 (2)	11 (2)
Sangre De Cristo	67 (4)	83 (5)	0 (0)	33 (2)	83 (5)	17 (1)	0 (0)	0 (0)	0 (0)
Nacimiento	83 (5)	83 (5)	0 (0)	67 (4)	100 (6)	83 (5)	0 (0)	0 (0)	0 (0)
Study Area Average	51 (44)	55 (47)	1 (1)	40 (34)	39 (33)	25 (21)	0 (0)	7 (5)	4 (2)

Changes in the length of the snowpack season, particularly the accumulation season, are less pronounced in the Front Range, Park Range and Flat Top Mountains (Table 4.2b). The percentage of stations showing a decline in these three areas are below to well below 44%. However, the percentage of warm days is increasing in approximately 92.5% of stations within the Front and Park Ranges (Table 4.2a). This overall temperature increase with little to no subsequent decrease in gross SWE indicates that losses in the max SWE, decreases in the length of the accumulation season, and earlier date of max SWE are primarily a function of increasing temperature. Additionally, increases in ablated SWE in 63% and 56% of stations within the Front and Park Ranges (Table 4.2a) implies that the slight increase in gross SWE is not resulting in a corresponding increase in the other snowpack season and SWE metrics, but is instead ablated by increasing temperatures. Losses in max SWE within the Flat Top Mountains are likely a function of both the increase in the percentage of warm days, measured in 40% of stations, and decreases in gross SWE, which was measured in 50% of the stations.

The Central Range, San Juan, Sangre de Cristo, and Nacimiento Mountains all indicate a decrease in the length of the accumulation season in over 62% of the stations measured (Table 4.2b). Additionally, all areas measured a decrease in the date of max SWE, indicating that the date of max SWE is measured earlier in the season in over 70% of the stations. Unlike the Front and Park Ranges, the gross SWE is showing statistically significant decreases in 50% and 83% of stations in the San Juan and Nacimiento Mountains respectively (Table 4.2b). This decline in total snowfall, combined with an increasing percentage of warm days in over 72% of the stations in the San Juan

Mountains and 100% of the stations in the Nacimiento Mountains, indicates that declining max SWE and shortening snowpack season metrics are a result of both temperature and precipitation. Declines in gross SWE within the Central Range and Sangre de Cristo Mountains are spatially less numerous than those within the San Juan and Nacimiento Mountains, with declines measured in 15% and 17% of stations respectively. Increases in the percentage of warm days measured in 55% and 100% of stations within the Central Range and Sangre de Cristo Mountains, combined with lower declines in gross SWE, indicate that declining max SWE, shortened snowpack season metrics, and earlier date of max SWE within these two areas are mainly a result of increasing temperature and larger magnitudes of ablated SWE.

Analysis of the study area indicates that 40% of the area is measuring a statistically significant decrease in the length of the snowpack season with 51% and 55% of stations showing a decline in the length of the accumulation season and an earlier date of max SWE respectively (Table 4.2b). An increase in the length of the ablation season in 18% of stations is likely a function of an earlier date of max SWE, with snowfall continuing to accumulate on the snowpack after the date of max SWE. Declines in the SWE metrics, snowpack metrics, and an earlier date of max SWE can be attributed to both increases in temperature and decreases in total snowfall. Increases in the percentage of warm days were measured in at least 79% of the stations, which has resulted in increased in ablation in 55% of the study area. In general, SWE and snowpack season metric declines are more attributable in increased temperatures in the northern mountain ranges, and a function of both increasing temperature and decreasing snowfall in the southern ranges.

4.2 SLR and RAP Analysis

Six dates were chosen for the SLR analysis of which at least one station measured 5.08 cm (2 in) of SWE and multiple stations measured >25.4 cm (10 in) of snow accumulation. The dates chosen for analysis in chronological order are: 11 May 2014, 16 Dec 2016, 22 Dec 2016, 1 Feb 2016, 9 Jan 2017 and 4 April 2017. The dates of these storms, ranging from December to May give a wide range of possible SLR's based upon the difference of winter (December – February) and spring (March –May) conditions. Events were also chosen to provide a wide geographic distribution for sounding locations. The stations chosen, total storm SLR and 3-hour accumulations are summarized in the Table 4.3. In total, 451 RAP generated soundings were created and analyzed for the analysis. SLR ranged from 0:0, or no measured precipitation, to 60:1. Of the 451 total 3-hour events, 306 events, or approximately 68%, had measured snowfall and SWE with a weighted mean SLR of 10.42:1. This is well below the climatological mean SLR for the region measured by Baxter et al. 2005 ranging from 14:1 to 16:1. A SLR of 10:1 had 107 events, or 35% of all events, with SLR above and below 10:1 accounting for 25% and 40% of events respectively (Figure 4.1). The SLR is likely lower than climatology for two reasons, compaction of the snowpack present prior to the event, and continual compaction of the snow accumulation during the event. Due to the wetness of the snow, with total storm SWE accumulations between 1.52 cm (0.6 inches) and 11.68 cm (4.6 inches), the weight of the snow snowfall likely compacted the existing snowpack and new snow accumulation as the storm progressed. This likely resulted in SLR's below the climatological mean; however, total storm SLR for the events on

Table 4.3. Summary of SWE and snowfall accumulations for dates chosen in SLR analysis.

Date	Station	Mountain Range	Elevation (m)	SWE/snow Accu. (cm)	Time (UTC) 00-03	03-06	06-06	09-12	12-15	15-18	18-21	21-00	00-03	03-06	06-09	Totals	SLR	Storm Mean/σ SLR
11 May 2014	Divide Peak, WY	Park	2706	SWE	0.0	0.0	0.3	0.8	0.5	1.5	1.0	0.5	0.3	0.0	0.3	5.08	10:1	11.3/2.0
				Snow	0.0	0.0	2.5	10.2	5.1	17.8	7.6	2.5	2.5	0.0	2.5	50.8		
	Burro Mountain, CO	Flat Top	2865	SWE	0.0	0.3	0.8	0.5	0.3	0.3	0.8	0.5	0.3	0.3	0.3	4.064	13:1	
				Snow	0.0	2.5	12.7	2.5	0.0	2.5	12.7	10.2	2.5	5.1	2.5	53.34		
	Bear Lake, CO	Front	2895	SWE	0.3	0.3	0.3	1.0	0.3	0.8	0.3	0.3	0.3	0.3	0.0	3.81	14:1	
				Snow	2.5	5.1	5.1	10.2	0.0	5.1	5.1	7.6	2.5	7.6	2.5	53.34		
	Sand Lake, WY	Front	3036	SWE	0.3	0.3	1.5	0.3	0.5	0.5	0.5	0.3	0.5	0.5	0.5	5.588	12:1	
				Snow	0.0	5.1	17.8	5.1	5.1	5.1	0.0	7.6	7.6	5.1	7.6	66.04		
	Elliot Ridge, CO	Central	3206	SWE	0.0	0.0	0.3	0.8	0.5	1.5	1.0	0.5	0.3	0.0	0.3	5.08	10:1	
				Snow	0.0	2.5	2.5	10.2	5.1	17.8	7.6	2.5	0.0	0.0	2.5	50.8		
	Schofield Pass, CO	Central	3261	SWE	0.3	0.3	1.0	0.8	0.8	0.3	0.5	0.5	0.0	1.0	0.3	5.588	9:1	
				Snow	2.5	2.5	12.7	2.5	5.1	2.5	2.5	5.1	0.0	10.2	2.5	48.26		
1 February 2016	Vacas Locas, NM	Nacimiento	2836	SWE	0.0	0.3	0.0	0.8	0.8	0.0	0.0	0.0	0.5	0.3	0.0	2.54	13:1	13.4/4.3
				Snow	0.0	2.5	0.0	7.6	5.1	0.0	0.0	2.5	5.1	7.6	2.5	33.02		
	Hopewell, NM	Nacimiento	3048	SWE	0.3	0.3	0.3	0.3	1.3	0.3	0.3	0.3	0.3	0.0	0.0	3.302	15:1	
				Snow	2.5	2.5	0.0	5.1	15.2	2.5	5.1	7.6	7.6	0.0	0.0	48.26		
	Brooklyn Lake, CO	Front	3121	SWE	0.0	0.0	0.3	0.0	0.0	0.5	0.3	0.0	0.3	0.3	0.0	1.524	22:1	
				Snow	0.0	0.0	2.5	0.0	0.0	7.6	15.2	0.0	5.1	2.5	0.0	33.02		
	Spud Mountain, CO	San Juan	3249	SWE	0.8	1.3	1.0	1.0	0.3	0.5	0.3	0.3	0.0	0.0	0.0	5.334	10:1	
				Snow	5.1	7.6	5.1	12.7	5.1	5.1	5.1	5.1	0.0	0.0	0.0	50.8		
	South Colony, CO	Sangre de Cristo	3292	SWE	0.5	0.8	1.3	0.3	1.0	0.8	0.0	0.0	0.0	0.0	0.0	4.572	8:1	
				Snow	2.5	5.1	7.6	2.5	7.6	10.2	0.0	0.0	0.0	0.0	0.0	35.56		
	Taos, NM	Sangre de Cristo	3370	SWE	0.3	0.3	0.8	0.3	0.8	0.8	0.0	0.0	0.0	0.0	0.0	3.048	13:1	
				Snow	2.5	2.5	7.6	2.5	10.2	12.7	0.0	0.0	0.0	0.0	0.0	38.1		
	Wesner Springs, NM	Sangre de Cristo	3389	SWE	0.0	0.3	0.5	0.8	1.0	0.3	0.3	0.0	0.3	0.0	0.0	3.302	13:1	
				Snow	0.0	2.5	5.1	7.6	15.2	2.5	2.5	0.0	5.1	0.0	2.5	43.18		
16 December 2016	Webber Springs, WY	Park	2819	SWE	0.3	0.8	0.8	1.3	1.3	1.0	0.5	0.8	0.0	0.0	0.0	6.604	7:1	7.5/2.2
				Snow	0.0	2.5	5.1	10.2	12.7	5.1	0.0	10.2	2.5	0.0	0.0	48.26		
	Bear Lake, CO	Front	2895	SWE	0.0	0.3	0.3	0.0	0.5	0.5	0.8	0.8	0.8	0.3	0.0	4.064	11:1	
				Snow	0.0	0.0	0.0	0.0	2.5	10.2	2.5	7.6	20.3	2.5	0.0	45.72		
	Park Reservior, CO	Central	3036	SWE	1.5	1.3	1.0	1.3	1.0	1.0	1.0	0.8	1.3	0.3	0.3	10.668	7:1	
				Snow	20.3	10.2	10.2	7.6	2.5	5.1	2.5	0.0	10.2	5.1	2.5	76.2		
	Hopewell, NM	Nacimiento	3048	SWE	0.0	0.3	0.3	0.8	0.8	1.0	0.8	0.3	0.5	0.8	1.3	6.604	6:1	
				Snow	0.0	0.0	2.5	5.1	5.1	5.1	5.1	2.5	0.0	2.5	10.2	38.1		
	Ripple Creek, CO	Flat Top	3151	SWE	0.3	0.8	0.3	0.5	1.3	1.0	0.3	1.5	1.3	0.3	0.3	7.62	8:1	
				Snow	2.5	7.6	2.5	7.6	5.1	7.6	0.0	10.2	17.8	2.5	0.0	63.5		
	Ivanhoe, CO	Central	3170	SWE	0.3	0.0	0.0	0.3	0.0	0.5	0.3	0.3	0.8	1.8	0.3	4.318	9:1	
				Snow	2.5	0.0	0.0	0.0	0.0	2.5	2.5	5.1	2.5	20.3	2.5	38.1		
	Schofield Pass, CO	Central	3261	SWE	0.8	0.5	0.5	1.0	1.3	1.5	1.5	1.0	1.0	1.8	0.8	11.684	6:1	
				Snow	5.1	5.1	2.5	7.6	7.6	10.2	5.1	2.5	2.5	22.9	2.5	73.66		
	Columbus Basin, CO	San Juan	3287	SWE	0.0	0.0	0.5	0.5	1.0	0.8	1.3	0.5	1.3	1.5	0.5	7.874	5:1	
				Snow	0.0	0.0	2.5	5.1	7.6	5.1	2.5	5.1	2.5	5.1	5.1	40.64		
	Wolf Creek Summit, CO	San Juan	3353	SWE	0.0	0.3	0.5	0.5	1.0	1.3	1.0	0.8	1.5	2.0	0.5	9.398	5:1	
				Snow	0.0	2.5	2.5	5.1	5.1	7.6	5.1	2.5	7.6	7.6	2.5	48.26		
	Loveland Basin, CO	Front	3475	SWE	0.0	0.0	0.0	0.3	0.0	0.5	0.3	0.5	1.0	0.5	0.3	3.302	11:1	
				Snow	0.0	0.0	0.0	2.5	0.0	5.1	2.5	2.5	15.2	7.6	0.0	35.56		
22 December 2016	Cascade #2, CO	San Juan	2719	SWE	0.0	0.0	0.3	0.3	0.5	0.3	0.3	0.3	0.3	0.3	0.3	2.54	12:1	7.8/2.6
				Snow	0.0	0.0	0.0	5.1	2.5	0.0	10.2	2.5	2.5	2.5	5.1	30.48		
	Vacas Locas, NM	Nacimiento	2836	SWE	0.0	0.0	0.5	0.5	0.5	0.5	0.8	0.0	1.0	0.3	0.0	4.064	6:1	
				Snow	0.0	0.0	2.5	5.1	2.5	0.0	5.1	2.5	5.1	2.5	0.0	25.4		
	Hopewell, NM	Nacimiento	3048	SWE	0.0	0.3	0.3	0.0	1.0	0.8	0.5	0.0	1.3	0.3	0.0	4.318	6:1	
				Snow	0.0	0.0	2.5	2.5	5.1	0.0	7.6	0.0	7.6	2.5	0.0	27.94		
	Culebra #2, CO	Sangre de Cristo	3200	SWE	0.0	0.0	0.3	0.0	0.8	0.5	0.8	0.3	0.5	0.8	0.3	4.064	10:1	
				Snow	0.0	2.5	5.1	5.1	5.1	2.5	5.1	2.5	5.1	2.5	5.1	40.64		
	Wolf Creek Summit, CO	San Juan	3353	SWE	0.0	0.0	0.0	0.5	0.8	0.5	0.8	1.0	1.0	0.8	0.5	5.842	7:1	
				Snow	0.0	0.0	0.0	5.1	5.1	2.5	7.6	2.5	15.2	2.5	2.5	43.18		
	Taos, NM	Sangre de Cristo	3370	SWE	0.0	0.0	0.3	0.5	1.0	0.8	1.8	0.3	0.8	0.8	0.0	6.096	6:1	
				Snow	0.0	0.0	2.5	2.5	5.1	5.1	7.6	2.5	5.1	5.1	0.0	35.56		
9 January 2017	Webber Springs, WY	Park	2819	SWE	0.5	0.5	0.3	0.0	1.0	2.0	1.3	0.5	0.8	0.3	0.0	7.112	6:1	8.1/2.7
				Snow	5.1	5.1	0.0	0.0	5.1	2.5	10.2	2.5	5.1	5.1	0.0	40.64		
	Joe Wright, CO	Front	3084	SWE	0.8	0.3	0.0	0.3	0.5	1.3	0.5	1.3	1.3	0.3	0.0	6.35	7:1	
				Snow	2.5	0.0	0.0	2.5	5.1	5.1	5.1	5.1	12.7	5.1	0.0	43.18		
	Ripple Creek, CO	Flat Top	3151	SWE	0.0	0.3	0.0	0.0	0.8	1.3	0.8	0.5	0.8	0.8	0.3	5.334	9:1	
				Snow	0.0	2.5	0.0	0.0	5.1	10.2	2.5	2.5	12.7	7.6	2.5	45.72		
	Copper Mnt, CO	Park	3215	SWE	0.3	0.0	0.0	0.0	0.0	0.5	0.0	0.3	0.8	1.0	0.0	2.794	13:1	
				Snow	2.5	0.0	0.0	0.0	0.0	7.6	0.0	5.1	10.2	10.2	0.0	35.56		
	Schofield Pass, CO	Central	3261	SWE	0.5	0.5	0.3	1.0	1.3	2.0	1.5	1.3	1.0	1.0	0.0	10.414	6:1	
				Snow	2.5	0.0	0.0	5.1	15.2	12.7	10.2	2.5	2.5	7.6	0.0	58.42		
	Columbus Basin, CO	San Juan	3287	SWE	0.0	0.0	0.0	1.3	0.8	1.5	1.3	0.8	0.8	0.3	0.3	6.858	6:1	
				Snow	0.0	0.0	0.0	5.1	10.2	7.6	7.6	2.5	5.1	2.5	2.5	43.18		
	Red Mountain Pass, CO	San Juan	3414	SWE	0.0	0.0	0.0	0.5	0.8	0.8	0.8	0.3	0.3	0.3	0.0	3.556	10:1	
				Snow	0.0	0.0	0.0	5.1	5.1	10.2	5.1	2.5	2.5	5.1	0.0	35.56		
4 May 2017	Vacas Locas, NM	Nacimiento	2836	SWE	0.0	0.0	0.3	1.0	1.3	0.3	0.0	0.0	0.0	0.0	0.0	2.794	10:1	12.4/2.7
				Snow	0.0	0.0	2.5	10.2	12.7	2.5	0.0	0.0	0.0	0.0	0.0	27.94		
	Idarado, CO	San Juan	2987	SWE	0.3	0.0	0.3	0.5	0.5	0.0	0.3	0.3	0.0	0.0	0.0	2.032	15:1	
				Snow	2.5	0.0	7.6	10.2	2.5	0.0	2.5	2.5	2.5	0.0	0.0	30.48		
	Apishapa, CO	Sangre de Cristo	3048	SWE	0.3	0.3	0.3	0.8	0.8	0.5	0.0	0.0	0.0	0.5	0.3	3.556	14:1	
				Snow	2.5	5.1	2.5	10.2	5.1	2.5	0.0	0.0	2.5	10.2	7.6	48.26		
	Joe Wright, CO	Front	3084	SWE	0.0	0.0	0.0	0.0	0.5	0.8	0.5	0.5	0.0	0.0	0.0	2.286	14:1	
				Snow	0.0	0.0	2.5	0.0	5.1	12.7	5.1	7.6	0.0	0.0	0.0	33.02		
	Hayden Pass, CO	Sangre de Cristo	3267	SWE	0.0	0.8	0.8	1.8	1.3	0.3	0.3	0.8	0.5	0.3	0.0	6.604	9:1	
				Snow	0.0	5.1	7.6	10.2	5.1	7.6	2.5	12.7	7.6	2.5	0.0	60.96		

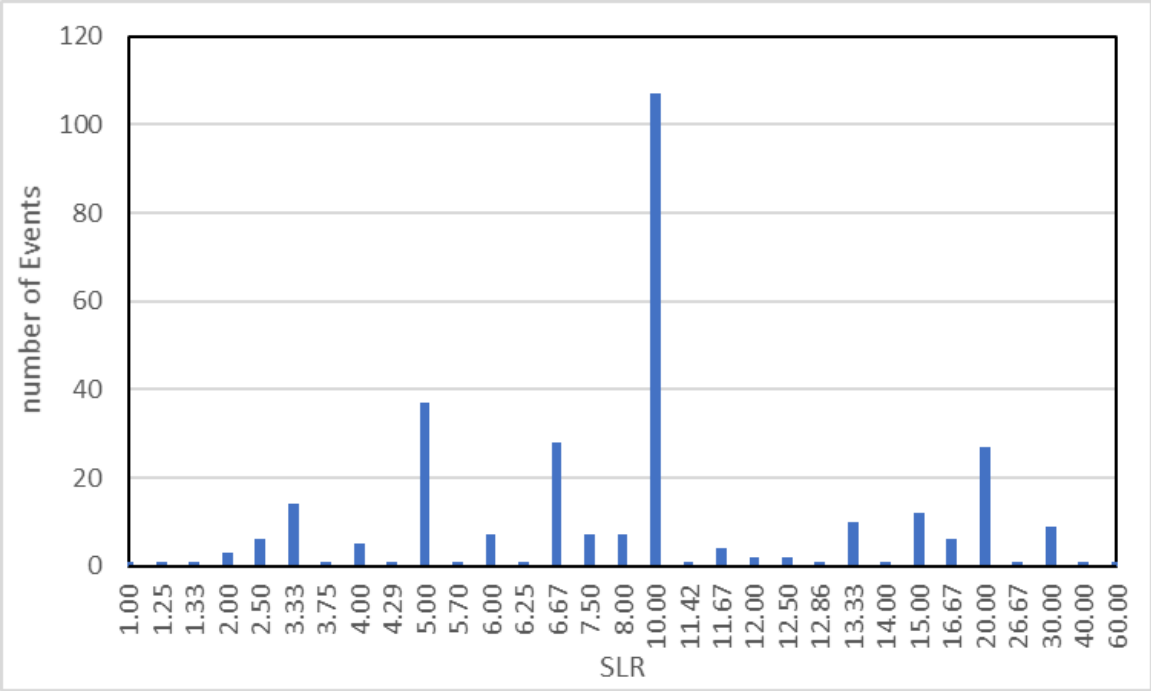

Figure 4.1. Total number of events by SLR.

11 May, 1 February, and 4 May were close to the lower bounds of the climatological average measured by Baxter et al. 2005, measuring approximately 11:1,13:1 and 12:1 respectively (Table 4.3). Large SLR values in short time increments, such as Wesner Springs on 1 February 2016 between 12 UTC and 15 UCT, measuring an SLR of approximately 15:1, keep the storm average SLR higher than those event dates that lack high SLR accumulations in a short period of time. This highlights the necessity of high snowfall magnitude over a short time period that is necessary to accurately resolve SLR using SNOTEL stations.

The coefficient of determination (R^2) was very low for the depth of all the major ice crystal growth layers for both the low DD and high DD thresholds throughout the study (Figure 4.2 – Figure 4.9). This is not surprising given the high variability in depth for a single SLR, especially SLR's with high frequency such as 5:1, 10:1, and 20:1. For

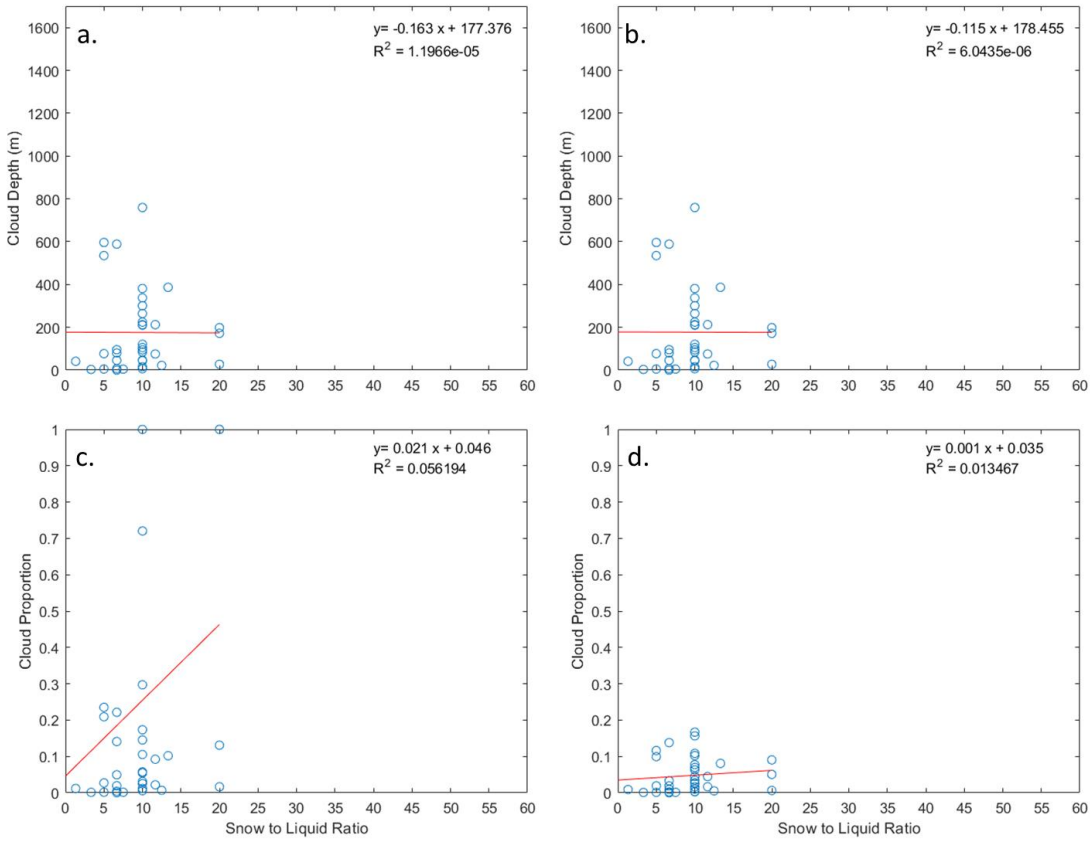

Figure 4.2. Depth and cloud proportion of the warm layer for (a,c) low and (b,d) high DD for SLR.

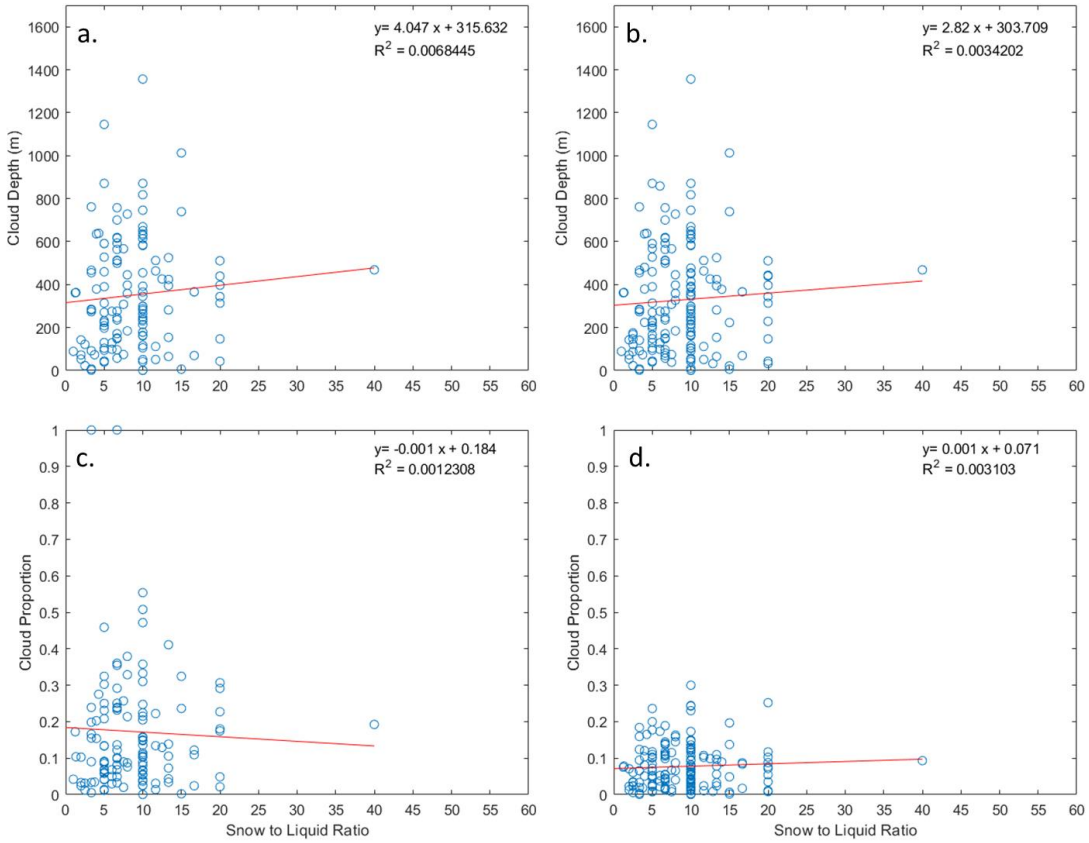

Figure 4.3. Depth and cloud proportion of the thick plate ice crystal growth layer for (a,c) low and (b,d) high DD for SLR.

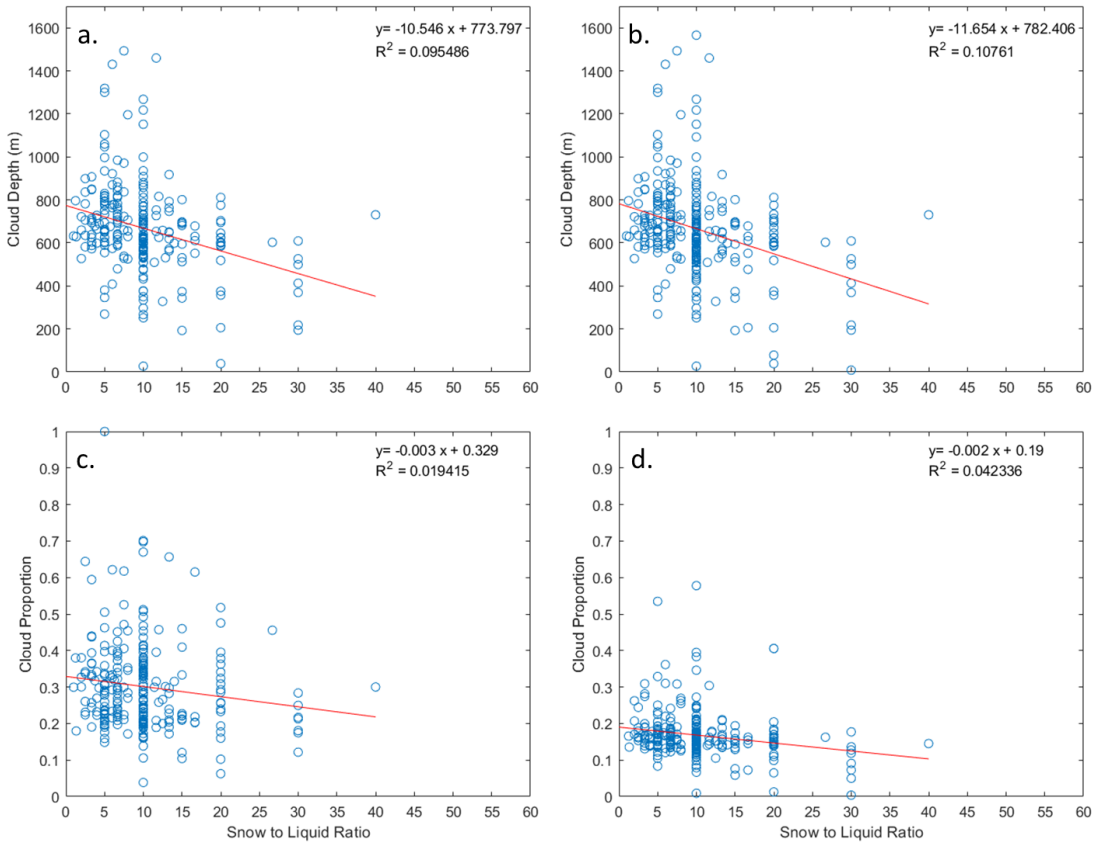

Figure 4.4. Depth and cloud proportion of the needle ice crystal growth layer for (a,c) low and (b,d) high DD for SLR.

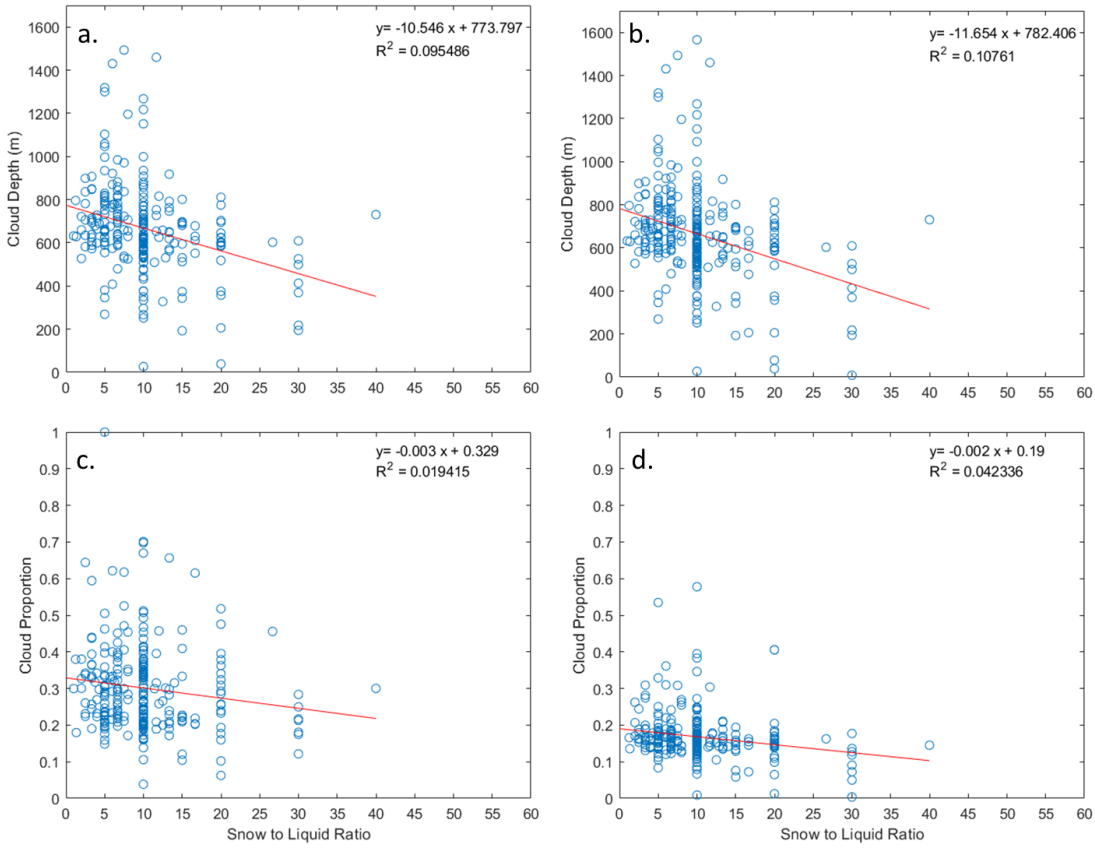

Figure 4.5. Depth and cloud proportion of the hollow column ice crystal growth layer for (a,c) low and (b,d) high DD for SLR.

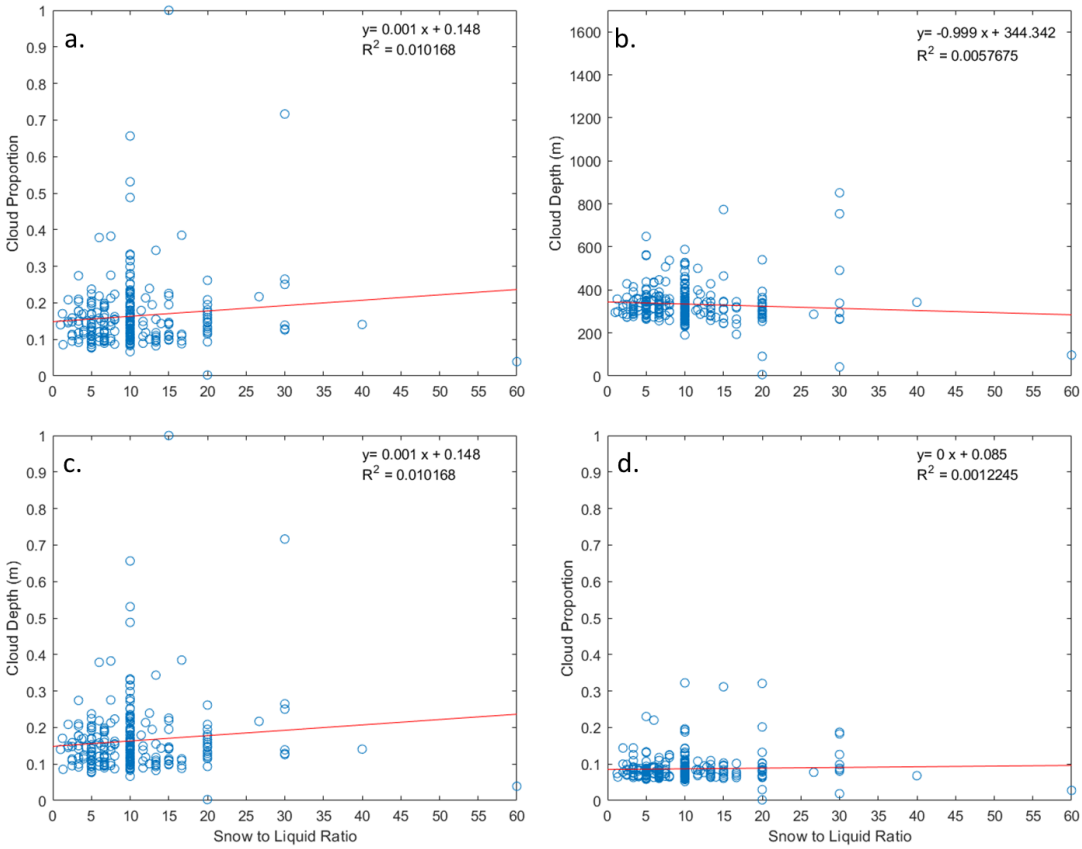

Figure 4.6. Depth and cloud proportion of the stellar plates ice crystal growth layer for (a,c) low and (b,d) high DD for SLR.

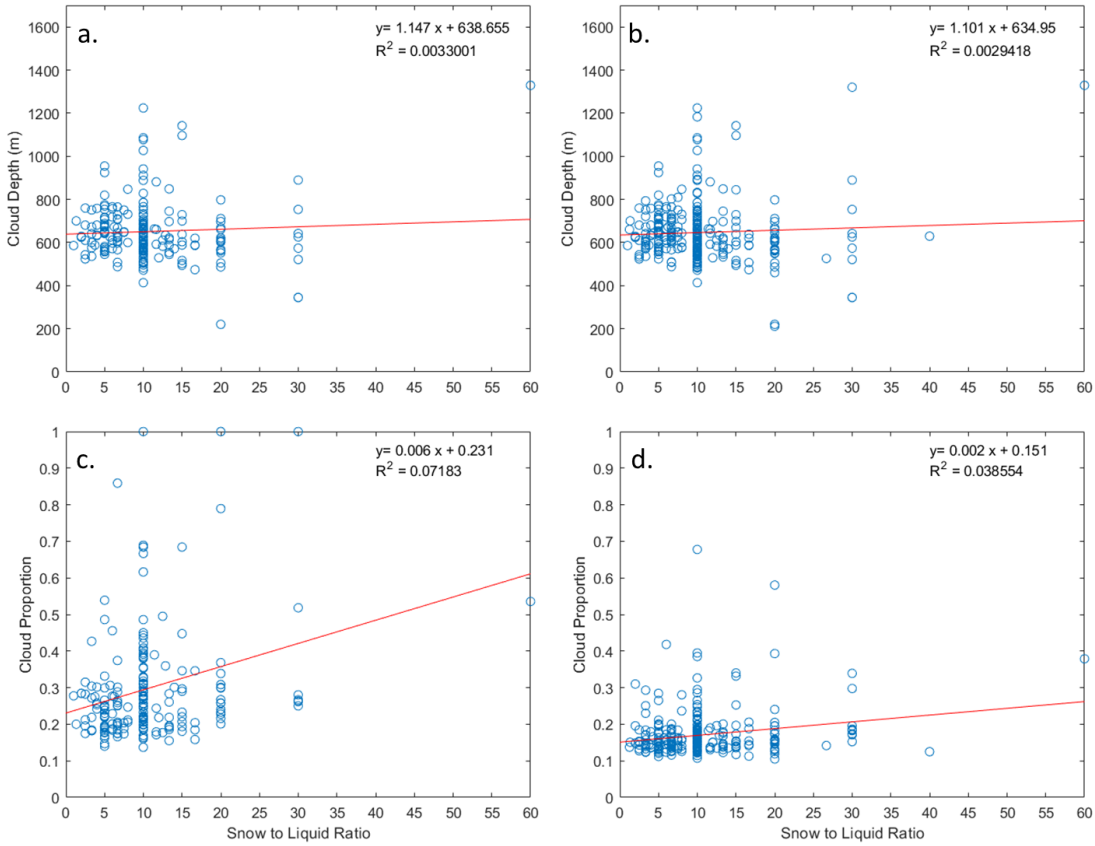

Figure 4.7. Depth and cloud proportion of the dendritic ice crystal growth layer for (a,c) low and (b,d) high DD for SLR.

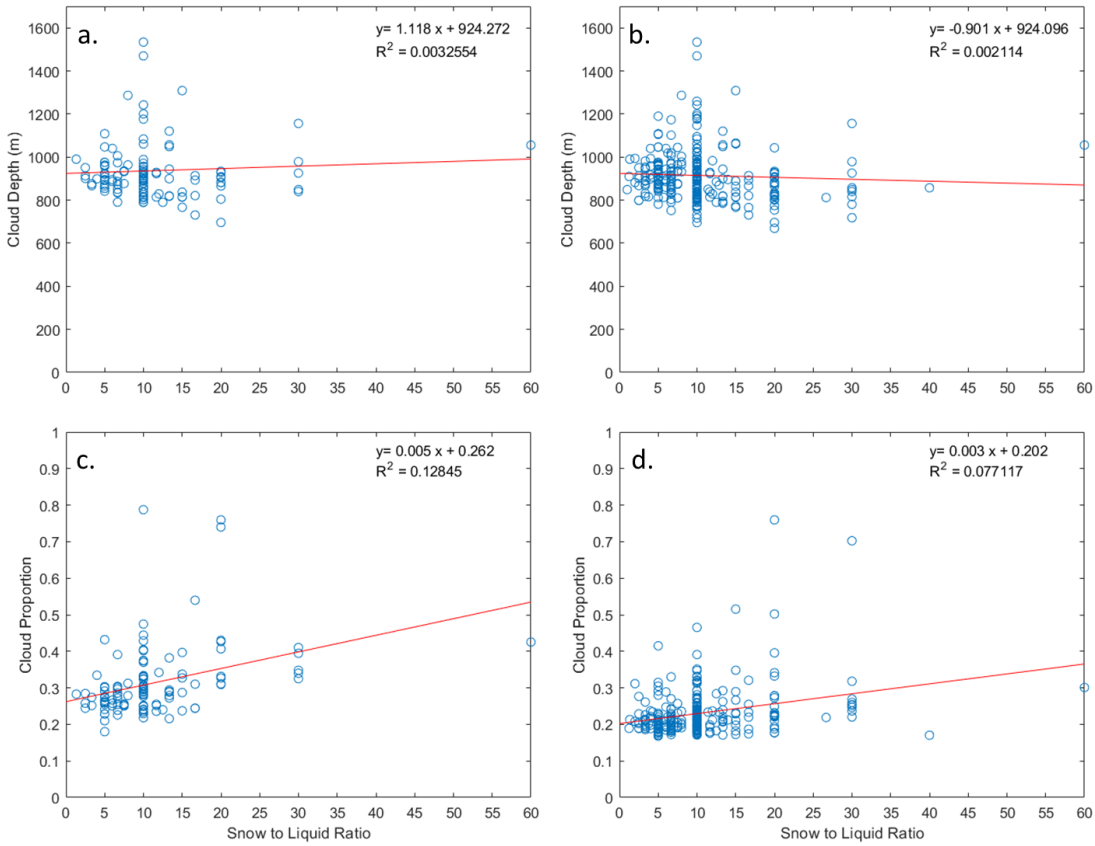

Figure 4.8. Depth and cloud proportion of the large plate ice crystal growth layer for (a,c) low and (b,d) high DD for SLR.

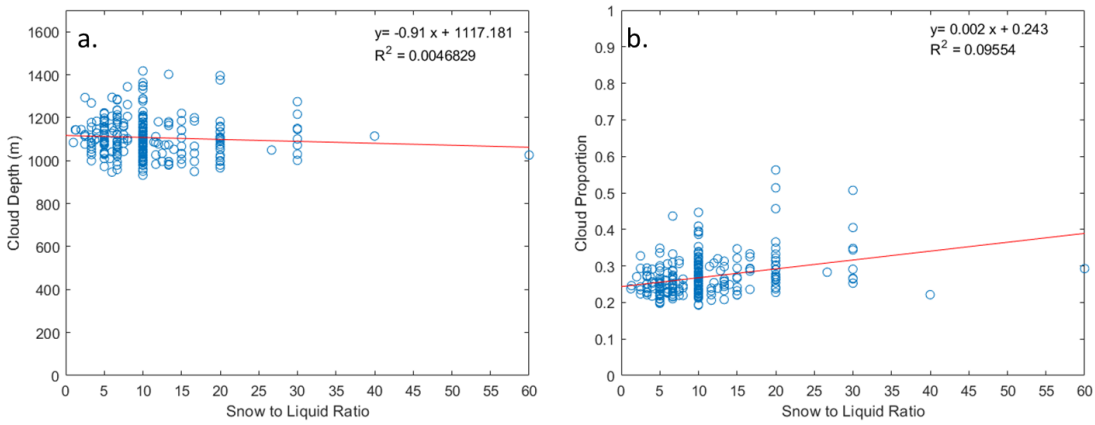

Figure 4.9. (a) Depth and (b) cloud proportion of the column ice crystal growth layer for SLR.

example, a 10:1 SLR within the needle ice crystal growth layer has 68 total events with a standard deviation of 241 m. Except for a few ice crystal growth layers, there is little differentiation, or slope, in the depth of the layer between the SLR categories. This is not surprising given that the possible range in depth for a given temperature layer has little ability to vary based on the confines of naturally observed lapse rates. With a few exceptions, most lapse rates will fall between the dry adiabatic and moist adiabatic lapse rate, meaning that a small variation of temperature in the vertical provides little variability in depth of the layer. However, there are a few instances where a lapse rate may become subadiabatic due to rapid vertical lift and high moisture content. Inversions due to advection of warm air into a crystal growth layer or rapid surface cooling may also increase the depth of crystal growth layers. Both features allow for the possibility that larger crystal growth layers may show a great enough variation in depth to differentiate between SLR categories.

The depth of the warm layer exhibited no clear trend in the depth-to-SLR relationship (Figure 4.2a,b). However, the presence of only 12% of total events containing this layer (Table 4.4) highlights that warm layers are often absent in orographic snowstorms, even within those containing a higher moisture content like the ones presented in this study. The high DD threshold was able to capture most of the events, with >90% of events represented within the hollow column, stellar plate, dendritic and large plate growth layers, thus highlighting that clouds with greater than approximately 65% relative humidity will tend to produce ice crystals within these layers. This can be attributed to the excess vapor pressure over ice with respect to water within these temperature regimes. The percentage of events captured using the low DD was less

Table 4.4. Number and percentage of events for the low and high DD thresholds by ice crystal type.

		# of Events		% of Events	
		Low DD	High DD	Low DD	High DD
Ice Crystal Growth Layer	Warm	36	36	12	12
	Thick Plates	128	164	42	54
	Needles	216	247	71	81
	Hollow Columns	254	292	83	95
	Stellar Plates	256	295	84	96
	Dendrites	205	298	67	97
	Large Plates	112	287	37	94
	Columns	0	266	0	87

than that of the high DD, although events containing the needle, hollow column, stellar plate, and dendritic growth layer were still represented in >67% of the events with measured snowfall.

The depth of the needle crystal growth layer, which is the densest ice crystal upon accumulation on the ground surface, shows a rapidly decreasing slope of approximately -10 m for each integer increase in SLR for both the low and high DD thresholds (Figure 4.4a,b). Although the R^2 is low for this analysis, it highlights that the SLR will tend to be lower with a greater cloud depth within this temperature range. Given that the temperature range for this ice crystal is between -3 °C and -6 °C, riming may also be increasing the density of the falling snow, and thus decreasing the SLR. A similar decrease in slope is present within the hollow column growth layer (Figure 4.5) with a R^2 value close to 0.1. Given that hollow column growth layer is also warmer than -10 °C, the same conclusions can be made as the needle growth layer. Within the

depth analysis, the needle and hollow column had the largest magnitude of slope and highest R^2 values, which could indicate the importance of these two layers in downward trending SLR with increasing depth due to both riming and the formation ice crystals that compact tightly upon accumulation at the ground surface.

Depth analysis of the warm and cold mixed phase ice crystal growth layer (Figures 4.10a,b and 4.11a,b) provides a larger range of possible depths for analysis due to a higher variation in lapse rates for the larger layers. The same trend of increasing depth for decreasing SLR can be seen in both the low and high DD thresholds for the warm mixed phase layer (Figure 4.10a,b). The slope of the regression for the warm mixed phase layer shows an approximately 31 m decrease for every integer increase in

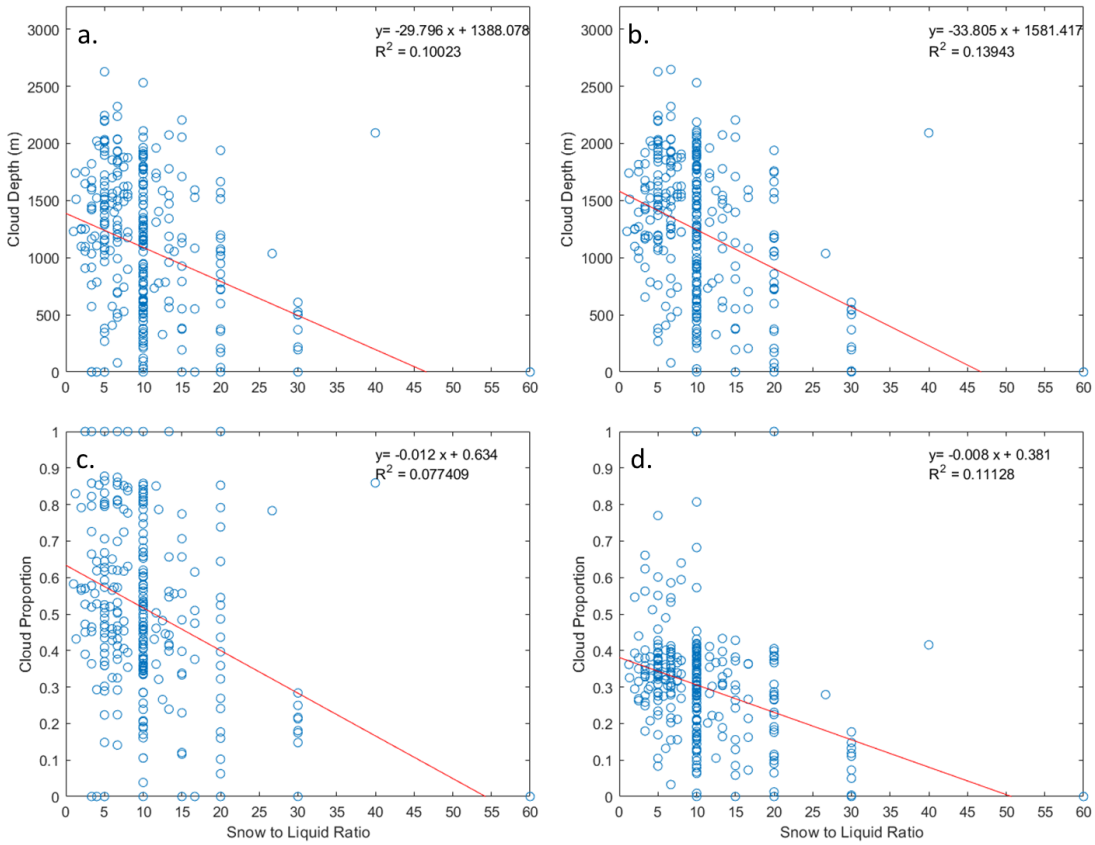

Figure 4.10. Depth and cloud proportion of the warm mixed phase ice crystal growth layer for (a,c) low and (b,d) high DD for SLR.

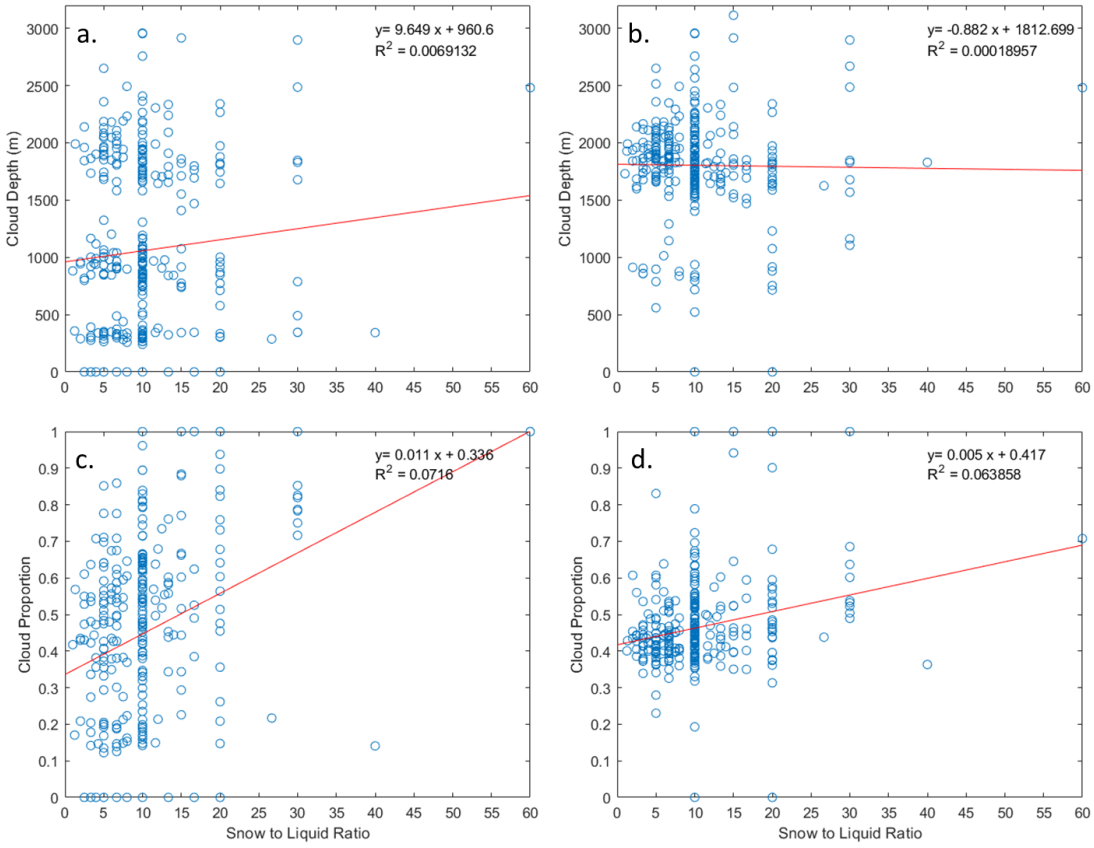

Figure 4.11. Depth and cloud proportion of the cold mixed phase ice crystal growth layer for (a,c) low and (b,d) high DD for SLR.

SLR for both the low DD and high DD thresholds. This indicates that the presence of thick plates, needles, hollow columns and a possible warm layer will tend to decrease the SLR with increasing depth. Given that this layer is warmer than -10 °C, there is also a higher likelihood that rimming will occur and lower the SLR as well. Within the cold mixed phase layer there is an increasing slope of the regression within the low DD threshold and close to no change for the high DD threshold (Figure 4.11a,b). Within the low DD threshold, the increasing depth of the cold mixed phase layer with increasing SLR indicates that the presence of less dense ice crystals, when accumulated on the ground, will tend to increase the SLR. However, the poor fit to the regression indicates that this trend is poorly resolved and will require further investigation.

Perhaps a more useful tool in differentiating SLR using the presence of ice crystal growth layers is the proportion of total cloud represented in each ice crystal growth layer since the variability in depth is highly regulated by lapse rates that can only vary by so much. Investigation of the cloud proportion for both the needles and hollow column growth layers shows the same decreasing slope in the regression (Figure 4.4a,b & 4.5a,b), similarly highlighting that the presence of these growth layers will tend to decrease the SLR due to higher likelihood of riming and dense ice crystals. Although the regression for the dendritic growth layer showed little change in the depth analysis (Figure 4.7a,b), the slope of the regression for cloud proportion shows an increase (Figure 4.7c) for the low DD threshold. This indicates that a higher proportion of the cloud within the layer responsible for the least dense ice crystals upon accumulation at the surface will tend to increase the SLR of the snowfall. Although the slope of the regression is lower in magnitude for the high DD, the same relationship is present (Figure 4.6d).

The large plate growth layer exhibits the same trend in increasing SLR for increasing cloud proportion (Figure 4.8c,d), thus indicating the presence of a large proportion of this cloud layer will tend to increase the SLR. This regression also has the largest R^2 value for the cloud proportion regression analysis (Figure 4.8c) despite a lower number of events containing this layer. Similar differentiation in cloud proportion is also apparent within the column growth layer (Figure 4.9b). Given that columns tend to be dense upon settling at the surface, the high proportion of the cloud within this layer for light SLR may seem contradictory. However, given the very low moisture content this high in the atmosphere, columns formed are likely lighter and less exposed to possible riming than columns that form within the hollow column growth layer lower in the

atmosphere, despite being hollow. Additionally, the proportion of cloud will be higher for larger SLR's within the column growth layer because the depth of the cloud tends to be lower for higher SLR events (Figure 4.12a,b).

The proportion of cloud for the warm and cold mixed phase layers (Figures 4.10c,d and 4.11c,d) shows the same relationship as the depth analysis (Figures 4.10a,b and 4.11a,b). This once again highlights that the presence of a large cloud proportion within the warm mixed phase layer, which contains dense ice crystals and a higher likelihood of rimming, will tend to decrease the SLR. The reverse trend is true for the cold mixed phase layer, with a higher cloud proportion within this layer tending to increase the SLR. By separating the moisture content of the cloud between the low and high DD thresholds there is clear increase in the cloud proportion for low SLRs within the warm mixed phase layer (Figure 4.10d,c). This may highlight the importance of using moisture as a threshold for determining SLR.

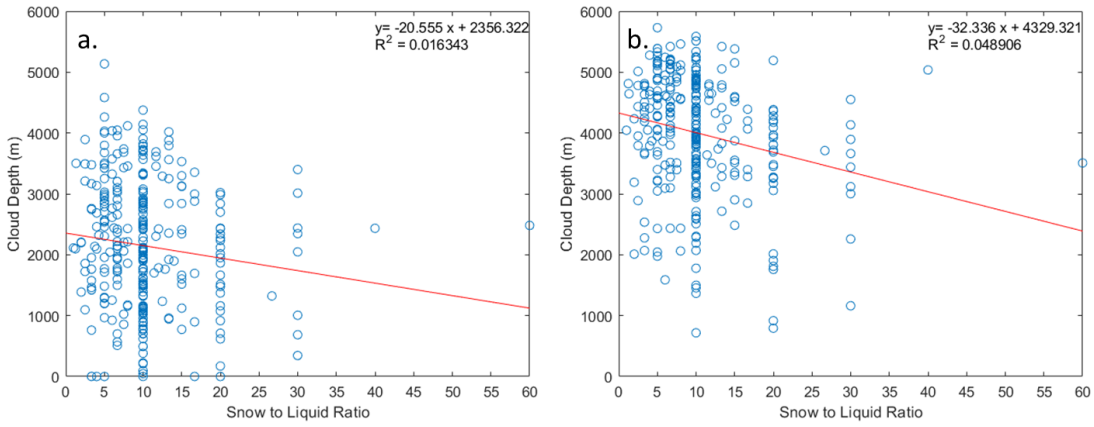

Figure 4.12. Total cloud depth for (a) low and (b) high DD for SLR.

CHAPTER 5: SUMMARY AND CONCLUSIONS

There were two primary goals to this study, to investigate tends in SWE metrics over time throughout the southern Rocky Mountains and to study relationships between crystal growth layers and SLR. The study area showed statistically significant negative r-values throughout many of the mountain ranges for snowpack season metrics and SWE metrics. These decreases show a continued decline in snowpack as seen in previous studies conducted by Clow (2009), Mote et al. (2004), and McCabe and Dettinger (2002). Additionally, statistically significant positive r-values in both the number of warm days and percentage of warm days were observed. The increase in these two temperature metrics have likely resulted in the increased ablation throughout the study area. However, implied increases in temperature and early snowpack conditioning for melt have not resulted in changes in the length of the ablation season apart from the Front and Park Ranges. The combination of an earlier date of max SWE and increases in gross SWE for both of these mountain ranges has likely lengthened the ablation season due to snowfall onto the snowpack that is ablating, thus extending the total length of the ablation season. The Central Range, San Juan, Sangre de Cristo, and Nacimiento Mountains, showed the largest percentage of stations measuring a decrease in the length of the accumulation season and an earlier date of max SWE. The Nacimiento Mountains showed the highest percentage of stations measuring decreases in all metrics other than the length of the ablation season, the number of warm days, and percentage of warm days. In general, SWE and snowpack season metric declines are more attributable to increased temperatures in the northern mountain ranges, and a function of both increasing

temperature and decreasing snowfall in the southern ranges. The decrease in snowfall in the southern mountain ranges is consistent with the study conducted by Hamlet et al. 2015. However, results from this study indicate increased ablation across the study area, highlighting the importance and attribution of increased temperature on declining snowpack. If declining trends were to continue, the availability of water late into the summer from snowmelt would likely decrease, especially within the southern areas of the study region which were measuring a higher proportion of stations with a declining trend.

Variability in SWE metrics and snowpack season metrics were high throughout the region. For example, the standard deviation in max SWE is as high as 21 cm and 27 cm for the Front and Park Ranges respectively. This is function of both the elevational differences between SNOTEL stations and the variability in total snowfall from year to year. Although there is a decreasing trend in max SWE throughout the study area, high year-to-year variability in SWE is likely to continue. A study conducted by Clow (2009) concluded that the duration of the ablation season has decreased throughout the western United States (Clow 2009). Results found in this study indicate that SNOTEL stations in the southern Rockies have yet to see this trend with only 5% of stations registering a statistically significant decrease in the length of the ablation season. This could be a function of station elevation, with the southern Rockies, particularly those within Colorado, having the highest elevation within the conterminous United Stations. High elevation allows for colder nocturnal temperatures in comparison to lower elevations, allowing snowpack to refreeze overnight during the ablation season, which decreases the speed at which snowpack can ablate. However, with an increase in the number and percentage of warm days, continual rise in temperature may cause a decrease

in the length of the ablation season if temperatures continue to increase from climate change as they are forecast to over the next century. However, this trend, at least for now, is not measured in the Front and Park Ranges due to increases in gross SWE and an earlier date of max SWE as discussed earlier. Increasing temperatures could also result in an increase in SWE or precipitation within the southern Rocky Mountains due to a higher moisture capacity within the air. Higher moisture content could therefore result in more intense cold season precipitation events, which could act to increase SWE if higher magnitude of precipitation were to offset increased losses to ablation. Regardless, changes in temperature and precipitation within the cold season of the southern Rocky Mountains will have an impact on the water resources within the region.

Building on the findings from this study, future work should focus on better methods of data gathering to provide a finer resolution of the atmospheric profile and better measurements for SLR and ice crystal type. This could be accomplished using soundings launched within mountainous terrain and using both SNOTEL stations and human observations of SWE and snow depth from the launch site. Continuous observation would still be required to eliminate the possibility of snow compaction. Cataloguing of ice crystals at the surface, or in cloud, would also aid in determination of ice crystal growth zones within orographic snowstorms. Expansion of this study could also be conducted using snowstorms with a lower requirement for SWE. Using the 5.08 cm threshold for 24-hour SWE accumulation likely skewed the results of this study towards lower SLRs. Reducing this threshold would likely yield results similar to the climatology presented by Baxter et al. 2005. Additionally, future work on the snowpack climatology will need to measure the magnitude of the temperature increase rather than

analyzing the number of days with a maximum temperature greater than 0 °C. Although the increase of the number and percentage of warm days was most pronounced in the Front and Park Ranges, days with only a few hours warmer than 0 °C will likely have little impact on the snowpack temperature structure. As a result, the magnitude of temperature, as well as the number of hours above 0 °C should be accounted for in future work.

SLR analysis relied on the assumption that the RAP model output correctly represented the atmosphere at the time of the analysis and that the SNOTEL station was correctly measuring the SWE and snowfall accumulation. Of course, numerical weather prediction is not always accurate, and the measurement and rounding errors of the SNOTEL stations may combine to misrepresent the true nature of the events. Since the snow accumulation is measured with a precision of 1.27 cm but reported to the nearest 2.54 cm, the results of the SLR analysis are likely inaccurate. Additionally, by using the SNOTEL network to infer SLR, snowpack compaction underneath the newly accumulated snow likely caused a disproportionately high number of low SLRs as compared to those measured in the SLR climatology by Baxter et al. 2005.

The assumption that ice crystal growth within each crystal growth layer is represented by only one crystal type is likely erroneous as well. However, results from this study allow one to infer that a high percentage of events that contained the dense needle and thick plate growth layers resulted in a lower SLR. Additionally, events were more likely to have average or light SLR's with the presence of the dendritic and large plate growth layers. These distinctions were more pronounced when using the low DD threshold compared to the high DD threshold, which could indicate the utility in

analyzing both the temperature and humidity profile to assess potential SLR's. However, using the depth of the crystal growth layers to differentiate SLR showed little distinction in SLR, with the slope of many regression curves being close to zero. This is not surprising given the small range of possible lapse rates within small temperature layers. Using cloud proportions for analysis showed that clouds with a higher proportion in temperatures colder than approximately -12 °C, corresponding with the dendritic growth layer, tended to have higher SLRs. Additionally, the total cloud depth tended to be smaller for higher SLRs, likely due to absence of a warm layer and a higher proportion of cloud within the colder temperatures. The potential to use this method as a tool for SLR forecasting should be investigated further.

REFRENCES

Albuquerque Business First, 2018: NM Ski Resorts off to a Fast Start, 11 November 2019, https://www.bizjournals.com/albuquerque/news/2018/12/03/nm-ski-resorts-off-to-a-fast-start.html

Alcott, T.I. and W.J. Steenburgh, 2010: Snow-to-Liquid Ratio Variability and Prediction at a High-Elevation Site in Utah's Wasatch Mountains. *Wea. Forecasting*, **25**, 323–337, https://doi.org/10.1175/2009WAF2222311.1 *Atmos. Sci.*, **66**, 2888-2899.

Avanzi, F., Hirashima, H., Yamaguchi, S., Katsushima, T., and De Michele, C., 2015: Observations of Capillary Barriers and Preferential Flow in Layered Snow During Cold Laboratory Experiments, *The Cryosphere*, **10**, 2013–2026, https://doi.org/10.5194/tc-10-2013-2016, 2016.

Bailey, M. and J. Hallett, 2004: Growth Rates and Habits of Ice Crystals Between -20° and -70°C. *J. Atmos. Sci*., **61**, 514–544.

Bailey, M. P., and J. Hallett, 2009: A Comprehensive Habit Diagram for Atmospheric Ice Crystals: Confirmation from the Laboratory, AIRS II, and other field studies. *J.*

Bark, R. H., Colby, B.G., and Dominguez, F. 2009: Snow days? Snowmaking adaptation and the future of low latitude, high elevation skiing in Arizona, 102, doi:10.1007/s10584-009-9708-x.

Baxter, M.A., C.E. Graves, and J.T. Moore, 2005: A Climatology of Snow-to-Liquid Ratio for the Contiguous United States. *Wea. Forecasting*, **20**, 729–744, https://doi.org/10.1175/WAF856.1

Benjamin, S., 2019: Diagnostic Output Fields for the Rapid Refresh and HRRR https://rapidrefresh.noaa.gov/RAP_var_diagnosis.html

Benjamin, S.G., S.S. Weygandt, J.M. Brown, M. Hu, C.R. Alexander, T.G. Smirnova, J.B. Olson, E.P. James, D.C. Dowell, G.A. Grell, H. Lin, S.E. Peckham, T.L. Smith, W.R. Moninger, J.S. Kenyon, and G.S. Manikin, 2016: A North American Hourly Assimilation and Model Forecast Cycle: The Rapid Refresh. *Mon. Wea. Rev.*, **144**, 1669–1694, https://doi.org/10.1175/MWR-D-15-0242.1

Cayan, D. R., 1996: Interannual Climate Variability and Snowpack in the Western United States. *J. Clim.*, **9**, 928–948, doi:10.1175/1520-0442(1996)009<0928:ICVASI>2.0.CO;2.

Clow, D. W., 2009: Changes in the Timing of Snowmelt and Streamflow in Colorado: A Response to Recent Warming. *J. Clim.*, **23**, 2293–2306, doi:10.1175/2009JCLI2951.1.

Colorado Ski Country USA, 2015: Economic Study Reveals Ski Industry's $4.8 Billion Annual Impact to Colorado, 11 November 2019, https://www.coloradoski.com/media_manager/mm_collections/view/183

Conway, H., and C. Wilbour, 1999: Evolution of Snow Slope Stability During Storms. *Cold Reg. Sci. Technol.,* **30,** 67–77.

Dawson, N., P. Broxton, X. Zeng, M. Leuthold, M. Barlage, and P. Holbrook, 2016: An Evaluation of Snow Initializations in NCEP Global and Regional Forecasting Models. *J. Hydrometeor.,* **17**, 1885–1901, https://doi.org/10.1175/JHM-D-15-0227.1

Durre, I., M.F. Squires, R.S. Vose, X. Yin, A. Arguez, and S. Applequist, 2013: NOAA's 1981–2010 U.S. Climate Normals: Monthly Precipitation, Snowfall, and Snow Depth. *J. Appl. Meteor. Climatol.,* **52**, 2377–2395, https://doi.org/10.1175/JAMC-D-13-051.1

Fukuta, N. and T. Takahashi, 1999: The Growth of Atmospheric Ice Crystals: A Summary of Findings in Vertical Supercooled Cloud Tunnel Studies. *J. Atmos. Sci.*, **56**, 1963–1979, https://doi.org/10.1175/1520-0469(1999)056<1963:TGOAIC>2.0.CO;2

Giorgio, N., 2017: Relation Between Cloud Cover and Relative Humidity. Institute for Marine and Atmospheric Research, Utrecht, **27**.

Hamlet, A.F., P.W. Mote, M.P. Clark, and D.P. Lettenmaier, 2005: Effects of Temperature and Precipitation Variability on Snowpack Trends in the Western United States. *J. Climate,* **18**, 4545–4561, https://doi.org/10.1175/JCLI3538.1

Judson, A. and N. Doesken, 2000: Density of Freshly Fallen Snow in the Central Rocky Mountains. *Bull. Amer. Meteor. Soc.,* **81**, 1577–1588, https://doi.org/10.1175/1520-0477(2000)081<1577:DOFFSI>2.3.CO;2

Knowles, N., M. D. Dettinger, and D. R. Cayan, 2006: Trends in Snowfall versus Rainfall in the Western United States. *J. Clim.*, **19**, 4545–4559, doi:10.1175/JCLI3850.1.

Marks D., Kimball J., Tingey D., and Link T., 1998: The Sensitivity of Snowmelt Processes to Climate Conditions and Forest Cover During Rain-on-Snow: a Case Study of the 1996 Pacific Northwest Flood, *Hydrol. Process.,* **12**, 1569-1587

McCabe, G.J. and M.D. Dettinger, 2002: Primary Modes and Predictability of Year-to-Year Snowpack Variations in the Western United States from Teleconnections with Pacific Ocean Climate. *J. Hydrometeor.*, **3**, 13–25, https://doi.org/10.1175/1525-7541(2002)003<0013:PMAPOY>2.0.CO;2

McCormick, H. S., 2009: *Observations and modeling of snow over the Washington Cascades*. Master's thesis, University of Washington.

Mote, P.W., A.F. Hamlet, M.P. Clark, and D.P. Lettenmaier, 2005: Declining Western Snowpack in Western North America. *Bull. Amer. Meteor. Soc.*, **86**, 39–50, https://doi.org/10.1175/BAMS-86-1-39

Nijssen, B., G.M. O'Donnell, D.P. Lettenmaier, D. Lohmann, and E.F. Wood, 2001: Predicting the Discharge of Global Rivers. *J. Climate*, **14**, 3307–3323, https://doi.org/10.1175/1520-0442(2001)014<3307:PTDOGR>2.0.CO;2

NOAA/NCEI, 2017: Rapid Refresh Analysis Collection 13km CONUS, continuing from May 2012 (updated daily). NCEI-NC THREDDS Server Archive, accessed 11 January 2019.

Oaida, C.M., J.T. Reager, K.M. Andreadis, C.H. David, S.R. Levoe, T.H. Painter, K.J. Bormann, A.R. Trangsrud, M. Girotto, and J.S. Famiglietti, 2019: A High-Resolution Data Assimilation Framework for Snow Water Equivalent Estimation across the Western United States and Validation with the Airborne Snow Observatory. *J. Hydrometeor.*, **20**, 357–378, https://doi.org/10.1175/JHM-D-18-0009.1

Pigeon, K., and Jiskoot, H., 2008: Meteorological Controls on Snowpack Formation and Dynamics in the Southern Canadian Rocky Mountains, *Arctic, Antarctic, and Alpine Research*, **40:4**, 716-730, https://doi.org/10.1657/1523-0430(07-054)[PIGEON]2.0.CO;2

Power, B. A., P. W. Summers, and J. d'Avignon, 1964: Snow Crystal Forms and Riming Effects as Related to Snowfall Density and General Storm Conditions. *J. Atmos. Sci.*, **21,** 300–305.

Rasmussen, R., B. Baker, J. Kochendorfer, T. Meyers, S. Landolt, A.P. Fischer, J. Black, J.M. Thériault, P. Kucera, D. Gochis, C. Smith, R. Nitu, M. Hall, K. Ikeda, and E. Gutmann, 2012: How Well Are We Measuring Snow: The NOAA/FAA/NCAR Winter Precipitation Test Bed. *Bull. Amer. Meteor. Soc.*, **93**, 811–829, https://doi.org/10.1175/BAMS-D-11-00052.1

Roebber, P.J., S.L. Bruening, D.M. Schultz, and J.V. Cortinas, 2003: Improving Snowfall Forecasting by Diagnosing Snow Density. *Wea. Forecasting*, 18, 264–287, https://doi.org/10.1175/1520-0434(2003)018<0264:ISFBDS>2.0.CO;2

Stoelinga, M.T., P.V. Hobbs, C.F. Mass, J.D. Locatelli, B.A. Colle, R.A. Houze, A.L. Rangno, N.A. Bond, B.F. Smull, R.M. Rasmussen, G. Thompson, and B.R. Colman, 2003: Improvement of Microphysical Parameterization through Observational Verification Experiment. *Bull. Amer. Meteor. Soc.*, **84**, 1807–1826, https://doi.org/10.1175/BAMS-84-12-1807

United States Department of Agriculture, Natural Resources Conservation Service, 2006: Land Resource Regions and Major Land Resource Areas of the United States, the Caribbean, and the Pacific Basin. U.S. Department of Agriculture Handbook 296, 682 pp. https://www.nrcs.usda.gov/Internet/FSE_DOCUMENTS/nrcs142p2_050898.pdf

United States Department of Agriculture, Natural Resources Conservation Service, 2018: Snow Telemetry (SNOTEL) and Snow Course Data and Products. Subset used: October 1979 – July 2018. National Water and Climate Center Data Archive, accessed July 2018, www.wcc.nrcs.usda.gov/snow.

United States Department of Agriculture, Natural Resources Conservation Service, 2017: Program history. Accessed 5 November 2019, https://www.wcc.nrcs.usda.gov/about/history.html

Vail Resorts, 2018: Vail Resorts Commits to $175 Million to $180 Million in Capital Investments to Reimagine the Guest Experience for the 2019-2020 Season, 11 November 2019, http://news.vailresorts.com/corporate/vailresorts/201920capital.htm

Wi, S., F. Dominguez, M. Durcik, J. Valdes, H. F. Diaz, and C. L. Castro, 2012: Climate Change Projection of Snowfall in the Colorado River Basin Using Dynamical Downscaling, *Water Resour. Res*., 48, W05504, doi:10.1029/2011WR010674.